Evaluation of cellular mechanisms for modulation of calcium transients using a mathematical model of fura-2 Ca^{2+} imaging in *Aplysia* sensory neurons

Hal Blumenfeld, Leonard Zablow, and Bernardo Sabatini
Center for Neurobiology and Behavior, Howard Hughes Medical Institute, Columbia University, New York, New York 10032 USA

ABSTRACT A theoretical model of $[Ca^{++}]_i$ diffusion, buffering, and extrusion was developed for *Aplysia* sensory neurons, and integrated with the measured optical transfer function of our fura-2 microscopic recording system, in order to fully simulate fura-2 video or photomultiplier tube measurements of $[Ca^{++}]_i$. This allowed an analysis of the spatial and temporal distortions introduced during each step of fura-2 measurements of $[Ca^{++}]_i$ in cells. In addition, the model was used to evaluate the plausibility of several possible mechanisms for modulating $[Ca^{++}]_i$ transients evoked by action potentials. The results of the model support prior experimental work (Blumenfeld, Spira, Kandel, and Siegelbaum, 1990. *Neuron.* 5: 487–499), suggesting that 5-HT and FMRFamide modulate action potential-induced $[Ca^{++}]_i$ transients in *Aplysia* sensory neurons through changes in Ca^{++} influx, and not through changes in $[Ca^{++}]_i$ homeostasis or release from internal stores.

INTRODUCTION

A number of theoretical models have been developed to describe the influx, diffusion, buffering, and extrusion of free intracellular calcium ($[Ca^{++}]_i$) in excitable cells (see Fischmeister and Horackova, 1983; Chad and Eckert, 1984; Sala and Hernandez-Cruz, 1990, for review). These models were developed for a variety of purposes, including analysis of the relationship between $[Ca^{++}]_i$ and transmitter release, $[Ca^{++}]_i$ and Ca^{++}-regulated ion channels, and $[Ca^{++}]_i$ and Arsenazo III signals. However, no previous model relates microscopic images recorded with the widely used $[Ca^{++}]_i$ indicator fura-2 (Grynkiewicz et al., 1985) to the actual temporal and spatial profile of $[Ca^{++}]_i$ in the cell. Such a model has been developed here, and is used for two purposes. First, it provides a multi-staged examination of the distortions inherent in fura-2 measurements of intracellular calcium. Second, we have used the model to simulate actual fura-2 measurements, and to test the plausibility of several mechanisms which have been proposed to modulate $[Ca^{++}]_i$ transients in experiments.

Distortions in fura-2 recordings can have an important impact on the biological conclusions reached from experiments. For example, how does the peak $[Ca^{++}]_i$ recorded with fura-2 correspond to the actual time and amplitude of peak $[Ca^{++}]_i$ in the cell? Can fura-2 reliably measure high speed changes in $[Ca^{++}]_i$ during action potentials? How are the amplitude and recovery time course of $[Ca^{++}]_i$ transients influenced by the intracellular fura-2 concentration? In order to address these and related questions we developed a model of the relationship between optical signals recorded with fura-2 and actual $[Ca^{++}]_i$. First, an idealized model was developed of calcium diffusion, buffering, and extrusion in *Aplysia* sensory neurons. Next, the kinetics of fura-2 and calcium binding were included in order to evaluate the temporal fidelity of fura-2 and to study the buffering effects of fura-2 itself. Finally, the measured optical properties of our recording system were incorporated in order to generate complete simulated photomultiplier tube (PMT) and video recordings of $[Ca^{++}]_i$. We were thus able to study the effects of nonconfocal microscope optics and other distortions introduced by the recording system. To assess the model's correspondence to a real cell we have compared the simulated $[Ca^{++}]_i$ measurements with experimental fura-2 recordings in *Aplysia* sensory neurons.

In *Aplysia* sensory-to-motor neuron synapses, transmitter release is facilitated by serotonin (5-HT) (Kandel and Schwartz, 1982) and inhibited by the peptide FMRFamide (Abrams et al., 1984). 5-HT increases action potential duration in sensory neurons by closing $S\text{-}K^+$ channels, thus indirectly increasing Ca^{++} influx (Klein and Kandel, 1978; Siegelbaum et al., 1982), while FMRFamide opens $S\text{-}K^+$ channels (Belardetti et al., 1987; Brezina et al., 1987) and also directly inhibits a component of Ca^{++} current (Brezina et al., 1987; Edmonds et al., 1990). These increases or decreases in Ca^{++} influx during action potentials result in corresponding changes in sensory neuron $[Ca^{++}]_i$ transients (Blumenfeld et al., 1990) which may be important for modulation of transmitter release from these cells (Hochner et al., 1986). Previous experiments suggest that 5-HT and FMRFamide modulate $[Ca^{++}]_i$ transients during action potentials entirely through changes in Ca^{++} influx (Blumenfeld et al., 1990). However, it has also been suggested that $[Ca^{++}]_i$ transients in these cells could be modulated through changes in $[Ca^{++}]_i$ buffering, transport, or release from intracellular stores (Boyle et al., 1984). Therefore, we have used the theoretical model to study the effects that each of these individual mechanisms should have on $[Ca^{++}]_i$ transients in *Aplysia* sensory neurons. We then ask which of these mechanisms can account for the effects observed experimentally with 5-HT and FMRFamide.

Address correspondence to H. Blumenfeld.

0006-3495/92/10/1146/19 $2.00

METHODS

The experimental setup and methods used here for measurement of $[Ca^{++}]_i$ with fura-2 have been described previously (Blumenfeld et al., 1990). Briefly, the fluorescence microscope system consisted of a 75 W Xenon arc lamp with a quartz condenser (Carl Zeiss, Inc., Thornwood, NY), a Zeiss IM35 inverted microscope with a quartz fluorescence intermediate piece and quartz nose piece and an Olympus UV Fluorite 40× objective (NA = 1.3). A 25% transmittance UV grade quartz neutral density filter (Omega Optical Inc., Brattleboro, VT) was used in the excitation pathway to minimize bleaching, and 340 and 380-nm bandpass filters (Andover Corp., Salem, NH) were positioned in the excitation light path by a motor which was controlled by the computer. The field diaphragm located in the fluorescence intermediate piece was used to restrict the excitation beam and was set at a diameter of 100 microns in the image plane. The filter block of the microscope contained a 395 nm dichroic mirror and an emission filter (Ditric Optics, Inc., Hudson, MA) with a center wavelength of 510 and 40-nm bandwidth at half-maximum transmittance. Emitted fluorescence light signals were measured either with a photomultiplier tube (PMT) (Schares Instruments; DCP-2), with a Hamamatsu SIT camera or a Hamamatsu intensified CCD camera (Bridgewater, NJ). A pinhole with variable aperture was used to measure light intensity with the PMT from different regions of the cell. The methods used for calibrations have been described previously, as have the methods used for cell culture and intracellular recording (Blumenfeld et al., 1990).

THE MODEL

1. Calcium diffusion

The cell body was represented by a sphere which was subdivided into N concentric shells, each having a thickness of Δr microns. The inner radius of shell n was taken to be $(n-1)\cdot\Delta r$ and the outer radius was $n\cdot\Delta r$. The concentrations of calcium, fura-2, and intracellular buffer were assumed to be constant within each shell. Calcium diffusion between shells was modeled using an adaptation of Fick's Law described by Chad and Eckert (1984). The diffusional flux of calcium entering shell n from shell $n+1$ is given by:

$$\left(\frac{\text{d mol of Ca}}{dt}\right)_{n+1\to n} = \frac{-D\cdot[Ca_n - Ca_{n+1}]\cdot 4\pi(n\Delta r)^2}{\Delta r}, \quad (1)$$

where D is the diffusion constant of calcium, Ca_n is the concentration of calcium in the nth shell, and Δr is the shell thickness. Then, since the volume of the nth shell is $(4/3)\pi\Delta r^3[n^3-(n-1)^3]$, the change in Ca_n will be:

$$\left(\frac{dCa_n}{dt}\right)_{n+1\to n} = \frac{-3D\cdot[Ca_n - Ca_{n+1}]\cdot n^2}{\Delta r^2\cdot[n^3-(n-1)^3]}. \quad (2)$$

A similar equation describes the diffusion from the $n-1$ shell to the nth shell, so that the total change in Ca_n is:

$$\frac{dCa_n}{dt} = \frac{3D\cdot\{(n-1)^2[Ca_{n-1} - Ca_n] - n^2[Ca_n - Ca_{n+1}]\}}{\Delta r^2\cdot[n^3-(n-1)^3]}. \quad (3)$$

The cell bodies of *Aplysia* sensory neurons have a radius of ~25 microns and this value was, therefore, used in the model. The shell thickness (Δr) was 1 μm, an acceptable value in terms of both stability of the solution and spatial resolution attainable with video microscopy. Smaller shell thicknesses were tested in the model as well, but these did not have any significant effects on the results on scales visible with current optical methods.

2. Calcium influx and calcium extrusion by membrane transport

Calcium influx was modelled as a rectangular pulse of current, i_{Ca}, entering uniformly throughout the external surface of the outermost shell, representing the cell membrane. Whole cell voltage clamp experiments with *Aplysia* sensory neurons give peak calcium currents of 2 to 5 nA (Edmonds et al., 1990) and a value of 3.9 nA (5×10^4 nA/cm^2) was, therefore, used in the model. Pulse duration was ordinarily 3 to 10 ms. Thus, the change in calcium concentration per second in the outermost shell (the Nth shell) due to calcium influx is:

$$\left(\frac{dCa_N}{dt}\right)_{\text{influx}} = \frac{3i_{Ca}}{8F\pi\Delta r^3[N^3-(N-1)^3]}. \quad (4)$$

Calcium extrusion was also assumed to occur uniformly throughout the cell membrane. The surface membrane pump in the model was intended to represent mechanisms such as Na/Ca exchange or the Ca^{++}-ATPase (Requena and Mullins, 1979; DiPolo and Beauge, 1983; Schatzmann, 1989; Blaustein, 1988; Barish and Thompson, 1983; Thayer et al., 1990). Although transport of Ca^{++} into endoplasmic reticulum probably plays an important role as well (Blaustein et al., 1978; Blaustein, 1988), this was not considered in the model. In squid, the relationship between $[Ca^{++}]_i$ and rate of Ca^{++} extrusion is fairly linear as long as $[Ca^{++}]_i$ does not exceed ~1 μM (Requena and Mullins, 1979; DiPolo and Beauge, 1983). In experiments in *Aplysia* sensory neurons the $[Ca^{++}]_i$ measured with fura-2 is well below 1 μM in all parts of the cell, and in the simulations below, $[Ca^{++}]_i$ in the outermost shell is also ordinarily below 1 μM, except for a very brief time during and just after the current pulse. Therefore, the calcium flux J_{Ca} (mol$\cdot$m$^{-2}\cdot$s^{-1}) through the cell membrane due to calcium pumping was modeled as:

$$J_{Ca} = \chi\cdot(Ca_N - Ca_r), \quad (5)$$

where Ca_N is the $[Ca^{++}]_i$ in the outermost shell, Ca_r is the resting $[Ca^{++}]_i$ (100 nM) and χ is a pumping constant with units of m$\cdot$s^{-1}. The second term of Eq. 5 is equivalent to a constant inward Ca^{++} leak of magnitude $\chi\cdot Ca_r$. Multiplying the flux given in Eq. 5 by the membrane surface area and dividing by the volume of the outermost

shell gives the change in calcium concentration per second in the outermost shell due to pumping:

$$\left(\frac{dCa_N}{dt}\right)_{pump} = \frac{-3\chi \cdot N^2 \cdot (Ca_N - Ca_r)}{\Delta r \cdot [N^3 - (N-1)^3]} = -P \cdot (Ca_N - Ca_r). \quad (6)$$

As in Zucker and Fogelson (1986) a value of 19.2×10^{-4} cm · s^{-1} was used for χ, yielding a value of 20 s^{-1} for P. Combining Eqs. 3, 4, and 6 gives:

$$\frac{dCa_N}{dt} = \frac{3D \cdot [Ca_{N-1} - Ca_N] \cdot (N-1)^2}{\Delta r^2 \cdot [N^3 - (N-1)^3]} + \left(\frac{dCa_N}{dt}\right)_{influx} + \left(\frac{dCa_N}{dt}\right)_{pump} \quad (7)$$

for the outermost shell.

3. Calcium binding with fura-2 and endogenous calcium buffers

As calcium diffuses through the cell body, it can be bound by both endogenous cellular buffers and the fura-2. The effect of buffers on calcium diffusion has been modeled previously in two different ways. In many models (e.g., Zucker and Stockbridge, 1983; Stockbridge and Moore, 1984) the effect of calcium buffering was incorporated by simply modifying the diffusion constant by a constant factor. These models assume that the calcium buffers do not diffuse and that the ratio of free to bound calcium remains constant throughout the $[Ca^{++}]_i$ transient. However, we were interested in including the effects of the diffusible buffer fura-2, and in modeling dynamic aspects of the $[Ca^{++}]_i$ transient for which equilibrium assumptions would not be valid. Therefore, as in Connor and Nikolakopoulou (1982) and others (Simon and Llinas, 1985; Gamble and Koch, 1987; Sala and Hernandez-Cruz, 1990) our model uses the unmodified calcium diffusion constant in aqueous solution (6.0×10^{-6} cm^2/s). We then simulate the effects of calcium binding to endogenous buffers and to the $[Ca^{++}]_i$ indicator fura-2 by using the following first order rate equations, with k_f and k_b representing forward and reverse rate constants:

$$\left(\frac{dCa_n}{dt}\right)_{buf} = k_{bbuf}[CaBuf_n] - k_{fbuf}[Ca_n][FreeBuf_n] \quad (8)$$

$$\left(\frac{dCa_n}{dt}\right)_{fura} = k_{bfura}[CaFura_n] - k_{ffura}[Ca_n][FreeFura_n]. \quad (9)$$

This approach gives the same results as the model of Zucker and Stockbridge at low time resolution and during the slow recovery phase of $[Ca^{++}]_i$ transients, but has the added advantage of being able to simulate effects due to fura-2 diffusion and due to rapidly changing $[Ca^{++}]_i$ as will be seen below.

Many different molecules in the cytoplasm can reversibly bind calcium, each one with its own rate constants and concentration (Carafoli, 1987; Blaustein, 1988). We have lumped these together as a single buffer (Buf above) with a forward rate constant (k_{fbuf}) of 10^8 M^{-1} s^{-1}, a reverse rate constant (k_{bbuf}) of 500 s^{-1}, a K_d(k_{bbuf}/k_{fbuf}) of 5 μM, and a buffer concentration of 153 μM. At a resting $[Ca^{++}]_i$ of 100 nM, this gives a ratio (β) of buffer-bound to free $[Ca^{++}]_i$ of 30. These values are consistent with the buffer capacity at rest measured in molluscan neurons by Ahmed and Connor (1988). Since most endogenous calcium buffers are large proteins, the buffer was considered to be immobile. The buffer was also assumed to be uniformly distributed throughout the cell, although some experiments have suggested nonhomogeneous calcium buffering in neurons (Tillotson et al., 1980).

In contrast to the endogenous buffers, both bound and free fura-2 are assumed to diffuse freely throughout the cell. The equations governing fura-2 diffusion are analogous to those presented above for calcium (Eqs. 1–3). For the diffusion constant of fura-2, we have used the in vitro value of 4.7×10^{-6} cm^{2}s^{-1} estimated by Timmerman and Ashley (1986) since the value in *Aplysia* cells is not known. The diffusion constant of fura-2 has been reported to be decreased by a factor of ~2 due to intracellular viscosity and binding in skeletal muscle cells (Timmermann and Ashley, 1986; Konishi et al., 1988) and neurons (Strautman et al., 1990; Adler et al., 1991). However, in smooth muscle cells (Williams et al., 1985) the mobility of fura-2 does not differ from its value in vitro. When the fura-2 diffusion constant in our model was reduced to 2.0×10^{-6} cm^{2}s^{-1}, the peak $[Ca^{++}]_i$ in the innermost shells occurred ~300 ms later due to slowed diffusion but, otherwise, the time course of $[Ca^{++}]_i$ during simulated transients was essentially unchanged.

The forward and reverse rate constant for calcium binding by fura-2 have been measured by Jackson et al. (1987) (see Table 1). The reverse rate constant of fura-2 was adjusted to give the appropriate K_d of 760 nM (Grynkiewicz et al., 1985) expected for the high ionic strength present in marine species. We estimated the intracellular fura-2 concentration in experiments to be 10–50 μM based on measurements done in the whole cell clamp configuration with known fura-2 concentrations in the patch pipette, and based on a comparison of fluorescence levels in fura-2 loaded cells to fluorescence of a microelectrode cuvette containing known fura-2 concentrations (see below).

In a recent $[Ca^{++}]_i$ diffusion model (Sala and Hernandez-Cruz, 1990; Hernandez Cruz et al., 1990) a second endogenous $[Ca^{++}]_i$ buffer which was freely mobile was included. For simplicity, we have used a single immobile cellular buffer, and were able to simulate the effects of mobile $[Ca^{++}]_i$ buffers by introducing varying concentrations of fura-2.

TABLE 1 **Model parameters**

Parameter	Value
Calcium	
Resting level	100 nM
Diffusion constant	6.0×10^{-6} cm^2/s
Current density	5×10^{-4} nA/cm^2
	= 3.9 nA/cell
Current pulse	10 ms, square pulse
Fura-2	
Total concentration	0–50 μM
K_d	760 nM
k_b	380/s
k_f	5×10^8/M·s
Diffusion constant	4.7×10^{-6} cm^2/s
Cellular buffer	
Total concentration	153 μM
K_d	5 μM
k_b	500/s
k_f	1×10^8/M·s
Pump	
Rate	P = 20/s
	$\chi = 19.2 \times 10^{-4}$ cm/s
Δt	
Rising phase	0.01 ms
Recovery phase	0.1 to 1.0 ms
Δr	1 μm
Cell radius	25 μm

4. Implementation of the model

Using the differential equations described above, the behavior of intracellular calcium in each shell can be determined by a numerical approximation in which time varies discretely in small steps (Δt). For each simulation the step size was chosen by reducing Δt until no significant change in the time-course of $[Ca^{++}]_i$ was detected. During the rising phase of $[Ca^{++}]_i$ transients and during the initial 100 ms of recovery a shorter Δt (0.01 ms) was generally needed than during the remainder of the recovery phase (Δt = 0.1 to 1.0 ms). The resting calcium ($Ca_n(t = 0)$) was 100 nM. With this approach, the concentrations of free calcium, free and bound intracellular buffer, and free and bound fura-2 can be determined at time $t + \Delta t$ from their respective values at time t by combining Eqs. 3, 8, 9 as follows:

From Eq. 10 it is clear that in order to determine $[Ca^{++}]_i$ for each shell at $t + \Delta t$ the free and bound buffer and fura-2 concentrations must also be calculated. This is done in Eqs. 11–14. In Eq. 13 the diffusion of $CaFura_n$ is modeled in the same way as the diffusion of free calcium described above (cf. Eqs. 3, 10). Free $Fura_n$ is also allowed to diffuse in the model. However, if it is assumed that bound and free fura-2 have the same diffusion constant then it can be proven inductively that the total fura-2 concentration in each shell will remain constant even when free and bound fura-2 diffuses from shell to shell. In this case the free fura-2 concentration can simply be calculated by subtraction, as is done in Eq. 14. Equations used for the outermost (Nth) shell were identical to Eq. 10–14 except that additional terms were present for calcium influx and pumping (Eq. 7).

Default values used in the model are found in Table 1. Except for where specifically mentioned, calcium diffusion was modeled using the "nonequilibrium" equations described above (8–14). During the rising phase of $[Ca^{++}]_i$ transients, large amounts of Ca^{++} influx and diffusion occur, and these "nonequilibrium" equations, therefore, provide an accurate portrayal of the rapid and dynamically changing $[Ca^{++}]_i$. However, as shown in Fig. 9*B*, during the recovery phase of $[Ca^{++}]_i$ transients the equilibration of $[Ca^{++}]_i$ with fura-2 and endogenous $[Ca^{++}]_i$ buffers occurs quickly in comparison to the rate of change of $[Ca^{++}]_i$. Thus, during the recovery phase the "nonequilibrium" model described above does not differ significantly from an "equilibrium" model in which the binding of Ca^{++} by fura-2 and endogenous buffers is assumed to reach equilibrium instantaneously within each Δt. In this case, the following equilibrium equations will hold for each shell:

$$\text{TotalFura} = \text{FreeFura} + \text{CaFura} = \text{CaFura} \cdot \left(1 + \frac{K_{\text{dfura}}}{\text{Ca}}\right) \tag{15}$$

$$\text{TotalBuf} = \text{FreeBuf} + \text{CaBuf} = \text{CaBuf} \cdot \left(1 + \frac{K_{\text{dbuf}}}{\text{Ca}}\right) \tag{16}$$

$$\text{Ca}_n(t + \Delta t) = \frac{3D_{\text{Ca}} \cdot \{(n-1)^2[\text{Ca}_{n-1}(t) - \text{Ca}_n(t)] - n^2[\text{Ca}_n(t) - \text{Ca}_{n+1}(t)]\}}{\Delta r^2 \cdot [n^3 - (n-1)^3]} \Delta t + \{k_{\text{bbuf}}[\text{CaBuf}_n(t)] - k_{\text{fbuf}}[\text{Ca}_n(t)] \times [\text{FreeBuf}_n(t)]\} \cdot \Delta t + \{k_{\text{bfura}}[\text{CaFura}_n(t)] - k_{\text{ffura}}[\text{Ca}_n(t)][\text{FreeFura}_n(t)]\} \cdot \Delta t + \text{Ca}_n(t) \tag{10}$$

$$\text{CaBuf}_n(t + \Delta t) = -\{k_{\text{bbuf}}[\text{CaBuf}_n(t)] - k_{\text{fbuf}}[\text{Ca}_n(t)][\text{FreeBuf}_n(t)]\} \cdot \Delta t + \text{CaBuf}_n(t) \tag{11}$$

$$\text{FreeBuf}_n(t + \Delta t) = \text{TotalBuf} - \text{CaBuf}_n(t + \Delta t) \tag{12}$$

$$\text{CaFura}_n(t + \Delta t) = \frac{3D_{\text{fura}} \cdot \{(n-1)^2[\text{CaFura}_{n-1}(t) - \text{CaFura}_n(t)] - n^2[\text{CaFura}_n(t) - \text{CaFura}_{n+1}(t)]\}}{\Delta r^2 \cdot [n^3 - (n-1)^3]} \Delta t - \{k_{\text{bfura}}[\text{CaFura}_n(t)] - k_{\text{ffura}}[\text{Ca}_n(t)][\text{FreeFura}_n(t)]\} \cdot \Delta t + \text{CaFura}_n(t) \tag{13}$$

$$\text{FreeFura}_n(t + \Delta t) = \text{TotalFura} - \text{CaFura}_n(t + \Delta t). \tag{14}$$

$$\text{TotalCa} = \text{Ca} + \text{CaFura} + \text{CaBuf}. \quad (17)$$

These equations (15–17) can be combined to give the following cubic equation:

$$0 = \text{Ca}^3 + \{K_{\text{dfura}} + K_{\text{dbuf}} + \text{TotalFura} + \text{TotalBuf} - \text{TotalCa}\} \cdot \text{Ca}^2 + \{\text{TotalFura} \cdot K_{\text{dbuf}} + \text{TotalBuf} \cdot K_{\text{dfura}} - \text{TotalCa} \cdot (K_{\text{dfura}} + K_{\text{dbuf}}) + K_{\text{dfura}} \cdot K_{\text{dbuf}}\} \cdot \text{Ca} - K_{\text{dfura}} \cdot K_{\text{dbuf}} \cdot \text{TotalCa}. \quad (18)$$

The real positive root of this cubic can easily be found (Bronsztejn and Siemiendiajew, 1959). Thus, in the equilibrium model, the new TotalCa for each Δt is first calculated by using Eq. (3) or (7). The new value for Ca is then calculated by solving (18) for each shell. With the above simplification, it is possible to run the model with much bigger values for Δt (up to 3–5 ms) without compromising stability or reliability of $[Ca^{++}]_i$ values during the decay phase.

GEOMETRICAL CONSIDERATIONS AND OPTICAL EFFECTS

The above equations provide a complete description of the three-dimensional $[Ca^{++}]_i$ profile elicited by calcium influx. The response of the model to a train of ten current pulses with two different fura-2 concentrations is shown in Fig. 1. In experiments, fura-2 recordings are typically performed either with a confocal or a standard fluorescence microscope coupled to a video camera or PMT. Therefore, rather than recording $[Ca^{++}]_i$ signals from throughout the volume of the cell as shown in Fig. 1, in experiments, fura-2 fluorescence signals are obtained from a single cross sectional slice through the cell, along with some out-of-focus light from above and below the focal plane. Two different methods for simulating $[Ca^{++}]_i$ measurements in a cross-sectional focal plane will now be described. First, we will describe $[Ca^{++}]_i$ for an ideal two-dimensional confocal slice through the cell. Then we will consider optical effects such as out-of-focus light and the effects of PMT pinhole selection on fura-2 recordings obtained with non-confocal fluorescence microscopy.

1. Ideal confocal cross section of $[Ca^{++}]_i$

Fig. 2 (*middle traces, A–D*) shows the time course of average $[Ca^{++}]_i$ in a cross-section through the center of the model cell in response to the same train of current pulses used in Fig. 1. In order to calculate the average $[Ca^{++}]_i$ in a cross-section, the contributions from each shell are weighted by $(2n - 1)/N^2$, i.e., the relative contribution of each shell to the cross sectional area (Fig. 2 *C, inset, darker symbols*). For comparison, the $[Ca^{++}]_i$ transient time courses generated by two other averaging methods are also shown (Fig. 2, *top* and *bottom traces, A–D*). When $[Ca^{++}]_i$ is averaged throughout the volume of the cell (*top traces*) each shell is weighted by $(3n^2 - 3n + 1)/N^3$, and the outermost shells, therefore, make a larger relative contribution than in the cross-sectional average (Fig. 2 *C, inset, lighter symbols*). Conversely, when $[Ca^{++}]_i$ is averaged along a radial line (*bottom traces*), as might be done by averaging values obtained along a single confocal microscope scan line, each shell is weighted equally by a factor of 1/25. Thus, with the radial average (*bottom traces*), the inner shells will contribute more heavily than with the cross-sectional average, and the peak $[Ca^{++}]_i$ value, therefore, occurs with a sub-

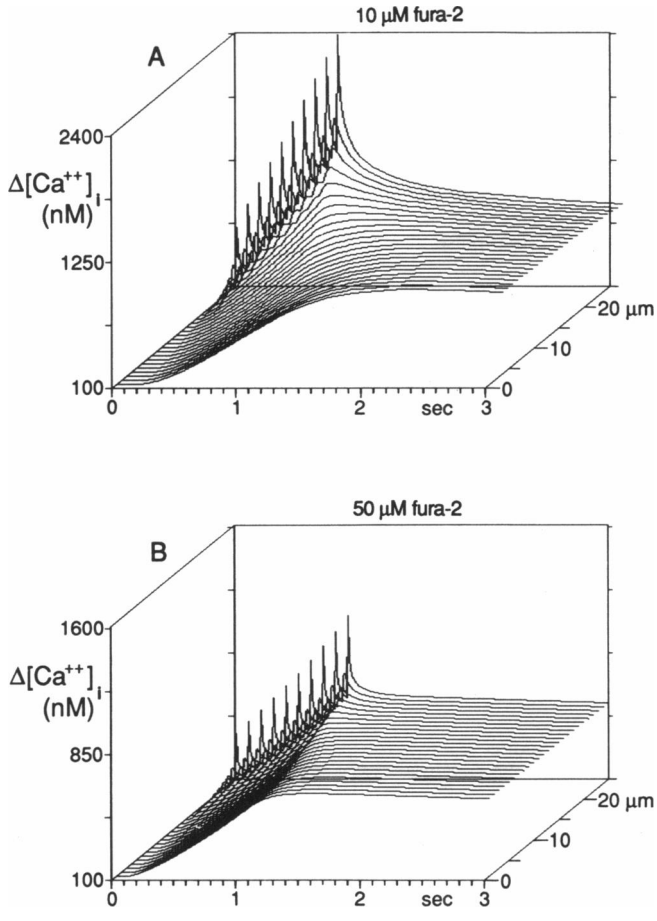

FIGURE 1 Free calcium concentration distribution predicted by the model during and after a 1.0 sec train of 10 ms rectangular current pulses given at 10 Hz. (*A*) 10 μM fura-2. (*B*) 50 μM fura-2. Fura-2 concentrations in experiments were estimated to lie between these two values. The traces shown deepest in the page are for shells closest to the cell membrane (25 μm) and the ones towards the front of the page are for the shells near the center of the cell (0 μm). The time courses for each of the 25 shells, spaced at 1-μm intervals, are shown. The stimulus begins at $t = 0$ and ends at $t = 0.9$ s. Peak $[Ca^{++}]_i$ for the innermost shell is at $t = 2.4$ s (*A*), and $t = 1.5$ s (*B*).

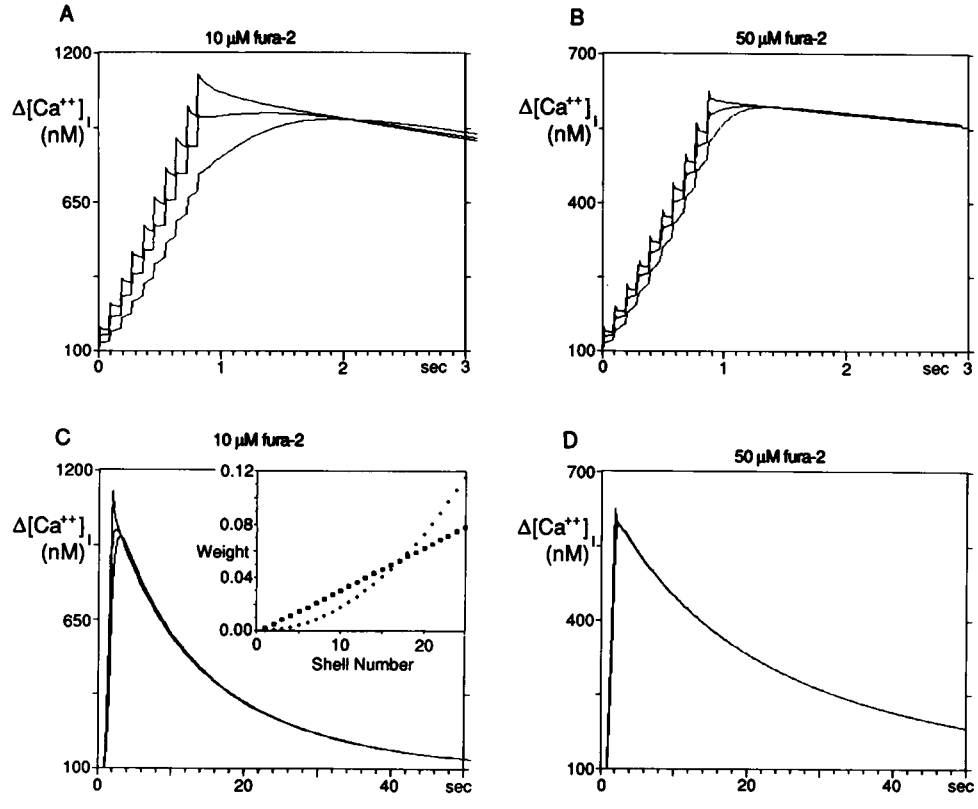

FIGURE 2 Simulated free calcium concentration averaged by three different methods. Same stimulus as in Fig. 1. Intracellular fura-2 concentrations are indicated. (*Top trace* in each panel) Volume average (weight of each shell is given by $(3n^2 - 3n + 1)/N^3$; see *inset*). (*Middle trace* in each panel) Average in cross section through center of cell (weight of each shell is given by $(2n - 1)/N^2$; see *inset*). (*Bottom trace* in each panel) Average along a radial line (each shell weighted equally). (*Inset*) Values of weighting functions used for cross sectional average (*darker symbols*) and volume average (*lighter symbols*).

stantial delay due to the time required for $[Ca^{++}]_i$ to diffuse toward the center of the cell. With the cross-sectional average (*middle traces*), the peak occurs earlier, but still with a significant delay of 0.7 s (Fig. 2, *A* and *C*) to 0.4 s (Fig. 2, *B* and *D*) from the end of the Ca^{++} current pulse. With the volume average (*top traces*), the peak $[Ca^{++}]_i$ coincides with the end of the current pulse and, consequently, with the peak $[Ca^{++}]_i$ in the outermost shells. These effects are less pronounced at the higher fura-2 concentration (Fig. 2, *B* and *D*) since $[Ca^{++}]_i$ then diffuses more quickly toward the center of the cell (Fig. 1). After the first few seconds, the time course of $[Ca^{++}]_i$ with the three different averaging methods converge (Fig. 2, *C* and *D*). This serves to illustrate that although the volume average of $[Ca^{++}]_i$ in the cell reaches its peak with the end of the current pulse, the average $[Ca^{++}]_i$ in a cross-section can continue to rise for a time due to geometric considerations alone. Another way of describing this is that the $[Ca^{++}]_i$ in cross-sections near the center of the cell will peak and decay slightly later than the volume average, while $[Ca^{++}]_i$ in cross-sections near the top and bottom surfaces of the cell will decay slightly more quickly than the volume average.

2. Effects of the optical microfluorescence system on fura-2 recordings

In order to evaluate the optical distortions introduced during fura-2 video or PMT recordings done with a nonconfocal microscope it was necessary to: (*a*) simulate the expected fura-2 fluorescence in response to the local calcium concentration throughout the cell, and to then (*b*) transform this signal in the same manner as our microfluorimetry system in order to generate complete images of $[Ca^{++}]_i$.

(*a*) Relationship between $[Ca^{++}]_i$ and fura-2 fluorescence signals

To simulate the response of fura-2 to calcium we needed to determine the relationship between free calcium and the absolute fluorescence levels of fura-2 at the excitation wavelengths used to measure $[Ca^{++}]_i$ (340 and 380 nm). According to Grynkiewicz et al. (1985) the fluorescence of fura-2 can be modelled as follows:

$$\text{Fluorescence at } 340 = F_1 = S_{b1}\text{CaFura} + S_{f1}\text{FreeFura} \quad (19)$$

$$\text{Fluorescence at } 380 = F_2 = S_{b2}\text{CaFura} + S_{f2}\text{FreeFura}. \quad (20)$$

Therefore, since values for $CaFura_n$ and $FreeFura_n$ are provided by the model (Eqs. 13 and 14), we needed to determine S_{b1}, S_{f1}, S_{b2}, and S_{f2} in order to calculate the fluorescence at 340 and 380 nm excitation wavelengths. This was done by measuring the fluorescence emitted by solutions with known concentrations of bound and free fura-2 (Blumenfeld et al., 1990) using 340 and 380 nm excitation wavelengths. Eqs. 19 and 20 could then be solved giving the following values for our recording system:

$$S_{b1} = 1.000; \quad S_{f1} = 0.455; \quad S_{b2} = 0.051; \quad S_{f2} = 1.006. \quad (21)$$

Since all calculations using these constants involve taking a ratio, only their relative magnitudes are important, and they have, therefore, each been normalized by S_{b1}.

(b) Point spread function of the microfluorescence system

By using the values from Eq. 21 in Eqs. 19 and 20 together with the model we were able to reconstruct the relative fluorescence intensities at 340 and 380 nm for each point within the cell. The next problem was to determine how our optical system transforms this three-dimensional ensemble of point sources of fluorescent light into a two-dimensional image detected by a PMT or video camera. In the specimen plane, an ideal fluorescent point source will pass through the microscope optics to produce an Airy disc (Inoue, 1986; Hecht and Zajac, 1974) in the image plane consisting of a small bright spot surrounded by progressively dimmer alternating light and dark concentric rings. If the specimen lay entirely in a two-dimensional plane, then its image would consist of the superposition of all the Airy discs produced by each individual point in the specimen plane. However, in a real specimen having finite thickness, there will also be contributions from point sources located above and below the specimen plane. Therefore, we needed to determine the image of a point source in focal planes both above and below the specimen plane, i.e., the point spread function (Inoue, 1986; Hecht and Zajac, 1974), for our optical system.

The point spread function was determined using digitized images of a fluorescent 0.2 μm polystyrene YG microsphere (Polysciences) taken at varying focal planes as described previously (Fay et al., 1986, 1989; Hiraoka et al., 1990). The microsphere diameter of 0.2 μm was smaller than the limit of resolution of the microscope ($\sim$0.24 μm). The point spread function obtained in this manner (Figs. 3, 4) implies that light from points beyond about 6 μm above or below the focal plane will contribute only a negligible amount to the fluorescence signal. The diameter of the field diaphragm (used to limit the region of illumination in the specimen plane) was 100 μm for these measurements, and for all fura-2 measurements done on cells. The emission optics used with the microspheres were identical to those used for fura-2. The excitation wavelength was 485 nm. Since this is longer than the 340 to 380 nm wavelengths used for fura-2 it is, therefore, expected to produce a point spread function which is slightly more spread out along the optical axis (Sheppard, 1988; Stokseth, 1969; Hopkins, 1955). Thus, these measurements of the point spread function actually provide an upper limit to the

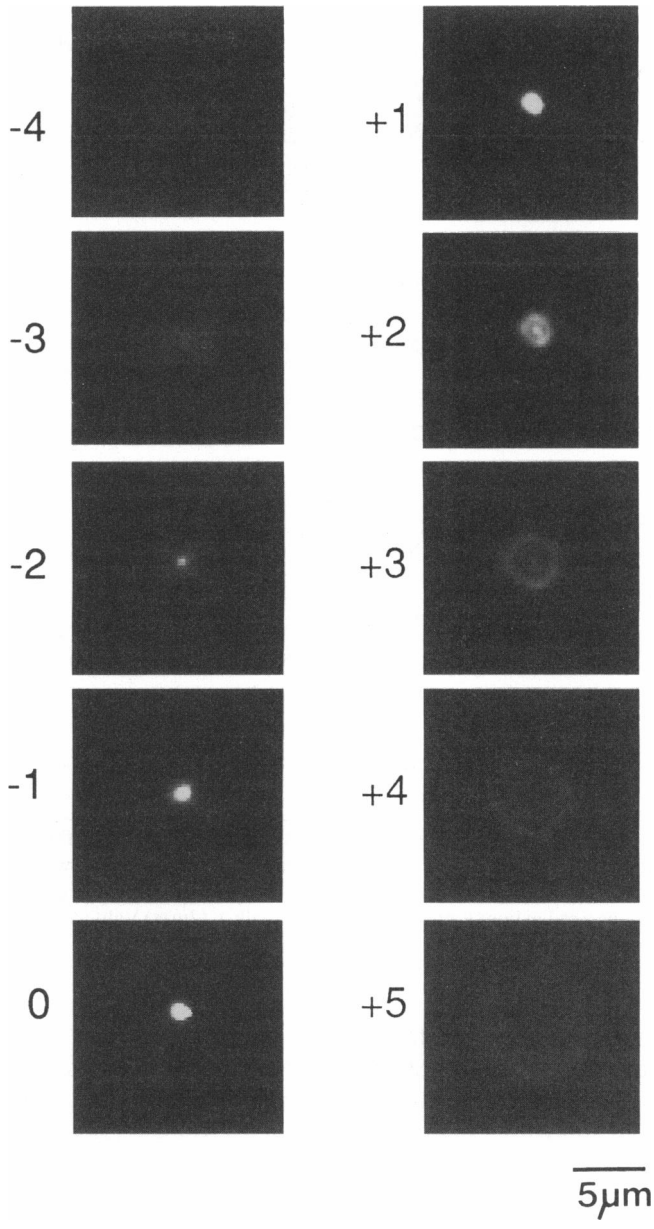

FIGURE 3 Point spread function of the fura-2 microfluorescence system. Images of a 0.2 μm fluorescent microsphere taken at different focal planes (indicated in microns). A dilute suspension of microspheres was evaporated onto a glass coverslip and images were then taken with a SIT camera (Hamamatsu) of an individual microsphere while adjusting the focus at 1-μm intervals. Focal planes acquired with the objective closer to the specimen are indicated by more positive numbers. Diameter of field diaphragm used to restrict the area of illumination was 100 μm in the specimen plane.

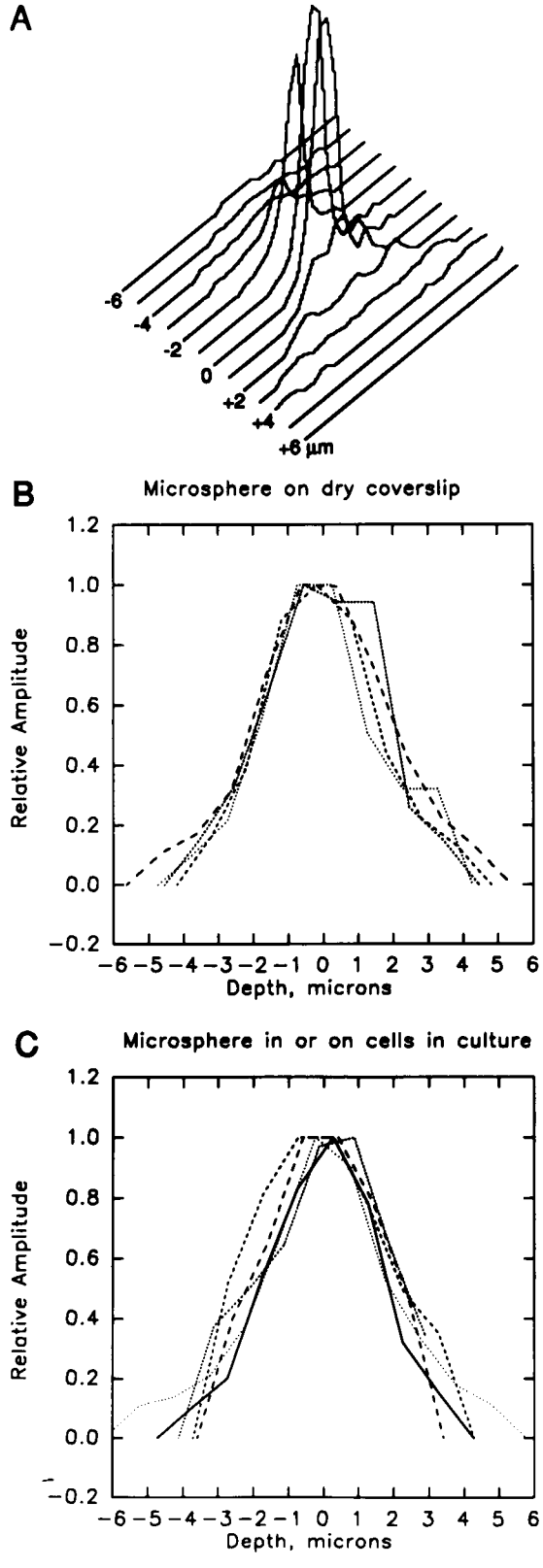

FIGURE 4 (*A*) Simplified point spread function assuming radial symmetry in planes perpendicular to the optical axis. Intensity values (*vertical axis*, arbitrary units) were obtained by scanning along a single line through the center of each of the successive digitized images shown in Fig. 3. Traces, from top left to bottom right, are from focal planes at −6, −5, −4, −3, −2, −1, 0, +1, +2, +3, +4, +5, +6 μm (more positive numbers indicate focal planes with the objective closer to the specimen). (*B*) Intensity drop-off (arbitrary units) as a function of defocus for point spread functions obtained with dry microspheres on glass cover slips ($n = 4$). Different microspheres indicated by different line types. (*C*) Intensity drop-off (arbitrary units) as a function of defocus for point spread functions obtained with microspheres on the surface of or within *Aplysia* sensory neurons in culture ($n = 5$). Different microspheres indicated by different line types.

extent of out-of-focus light present in fura-2 measurements.

In addition to nonconfocal microscope optics, a second effect which could potentially introduce stray light into the recorded image in a biological specimen is light scattering. Therefore, we added a dilute suspension of microspheres to five culture dishes containing *Aplysia* sensory neurons, allowed them to settle for 3–4 h, and then exchanged the solution in the dishes with fresh medium in order to remove the microspheres still in suspension. Upon imaging these cells under the same conditions used above, fluorescent microspheres were seen on the surface of the cells, and by focusing up and down it appeared that some microspheres were present within the cells as well. The point spread functions obtained with these microspheres were not significantly different from those obtained above with dry microspheres on plain glass (Fig. 4, *B* and *C*). Thus, it appears that light scattering due to cytoplasm and culture medium does not significantly change the point spread function measured under the conditions used for our experiments.

Using the point spread function as determined above, we could generate images of any focal plane or cross section in our model cell. The intensity at each point in the image was calculated by adding up the contributions (given by the point spread function) of all the points in the volume surrounding that point in the model cell. This is equivalent to performing a discrete approximation to the convolution integral of the fluorescence intensity in the cell and the point spread function in order to obtain an image at a particular focal plane. Images were generated in this way for both 340 and 380 nm excitation wavelengths.

(c) Simulation of fura-2 video recordings

$[Ca^{++}]_i$ is measured with fura-2 by taking the ratio of images at 340 and 380 nm excitation wavelengths. The relationship between these ratio values (R) and $[Ca^{++}]_i$ is then estimated through calibration measurements which can be fit by the following equation (Grynkiewicz et al., 1985):

$$[Ca^{++}]_i = K_{dfura}\left(\frac{R - R_{min}}{R_{max} - R}\right)\left(\frac{S_{f2}}{S_{b2}}\right), \qquad (22)$$

where R_{min} is the ratio value as $[Ca^{++}]_i$ approaches zero, R_{max} is the ratio value at saturating $[Ca^{++}]_i$ and S_{f2} and S_{b2} have been defined above.

In a simulation of fura-2 video recordings, a point by point ratio was taken of images generated at 340 and 380 nm for a focal plane through the center of the cell, which is the focal plane which was routinely used in our experiments. The resulting maps of 340/380 ratios were then converted into complete simulated images of $[Ca^{++}]_i$ by using Eq. 22, together with values for R_{min}, R_{max}, and $K_{dfura}(S_{f2}/S_{b2})$ determined by calibration measurements (Blumenfeld et al., 1990). Since $[Ca^{++}]_i$ does not approach R_{max} of the fura-2 calibration curve in experiments or even in the outermost shells of the simulations below, there is probably no significant problem with saturation of the fura-2 response in these cells.

We were interested in estimating the distortion introduced into fura-2 images by out-of-focus light. Therefore, we compared the time course of average $[Ca^{++}]_i$ predicted above (Fig. 2) for an ideal confocal cross section to the time course of average $[Ca^{++}]_i$ in simulated images which include the convolution operation. As seen by comparing the top and middle traces in Fig. 5 *A*, the convolution operation has only a very small effect on the time course of $[Ca^{++}]_i$. Similarly, video-like images of the spatial profile of $[Ca^{++}]_i$ varying over time were only minimally affected by the convolution operation, especially for focal planes near the center of the model cell (data not shown). Thus, according to the model, video images of $[Ca^{++}]_i$ measured using fura-2 with the microscope focused on a plane through the center of the cell, and using a relatively small field diaphragm (100 μm) as was used here, should provide a fairly accurate representation of $[Ca^{++}]_i$ in a cross-sectional plane.

(*d*) Simulation of fura-2 PMT recordings

When fura-2 measurements are performed with a photomultiplier tube (PMT) a pinhole having a projected diameter of several microns in the specimen plane is typically used. Thus, the fluorescence from different locations within the pinhole is effectively averaged at each wavelength prior to taking the ratio. In order to understand how this averaging, and how the location of the pinhole on the cell alters the observed free calcium values, we simulated the effects of the pinhole with our model. This was done by starting with the 340 and 380-nm images generated by the convolution operation, and separately averaging the fluorescence within a circular pinhole for each wavelength. The ratio of the 340 over 380 nm signal was then used to calculate free calcium with Eq. 22.

In order to evaluate the distortion due to spatial averaging, a worst-case scenario was assumed, where the PMT pinhole diameter was 50 μm and would, therefore, include the entire model cell. In this case, there was a small damping effect on the contribution of the outermost shells to the signal during the rising phase as shown in Fig. 5 *A* (*bottom trace*). There was no effect, however, on the peak amplitude of the $[Ca^{++}]_i$ transient, on the time course of $[Ca^{++}]_i$ following the peak, or on the delay between the end of the current pulse and the $[Ca^{++}]_i$ transient peak. On longer timescales, such as that used in Fig. 2, *C* and *D* no significant difference can be detected between $[Ca^{++}]_i$ transients simulated by the three different methods used in Fig. 5 *A*.

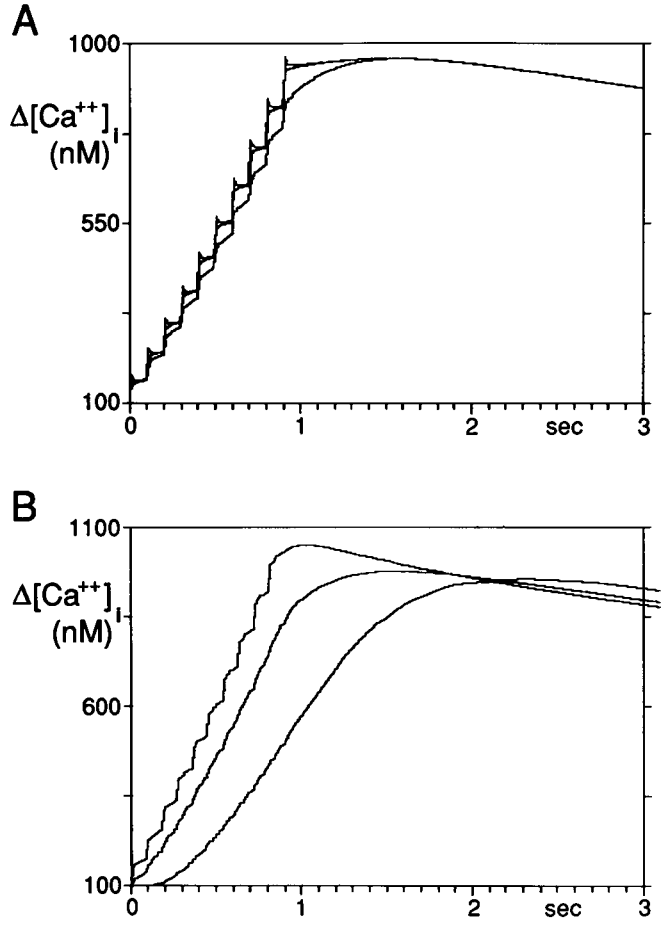

FIGURE 5 Complete simulated fura-2 video and PMT measurements of $[Ca^{++}]_i$. Stimulus was a train of ten current pulses (pulse duration = 10 ms; frequency = 10 Hz). Fura-2 concentration = 10 μM. (*A*) (*Top trace*) Average $[Ca^{++}]_i$ predicted by the model in a cross section through the center of the cell without incorporating the optical transfer function (same as Fig. 2 *A*, *middle trace*). (*Middle trace*) Simulation of average $[Ca^{++}]_i$ in video images taken in a focal plane through the center of the cell. (*Bottom trace*) Simulation of PMT measurements of $[Ca^{++}]_i$ taken in a focal plane through the center of the cell with the pinhole aperture covering the entire cell. Similar results are seen with 50 μM fura-2. (*B*) Effect of pinhole position on simulated PMT measurements. Pinhole radius = 8 μm. (*Left trace*) Center of pinhole at 19 μm from middle of cell. Peak $[Ca^{++}]_i$ occurs 200 ms after end of current pulses. (*Middle trace*) Center of pinhole at 15 μm from middle of cell. Peak $[Ca^{++}]_i$ occurs 700 ms after end of current pulses. (*Right trace*) Pinhole centered on middle of cell. Peak $[Ca^{++}]_i$ occurs 1.5 s after end of current pulses.

A second aspect of PMT measurements that was explored with the model was the effect of pinhole position (Fig. 5 *B*). For these simulations, a pinhole with a radius of 8 μm in the specimen plane was used, which is the

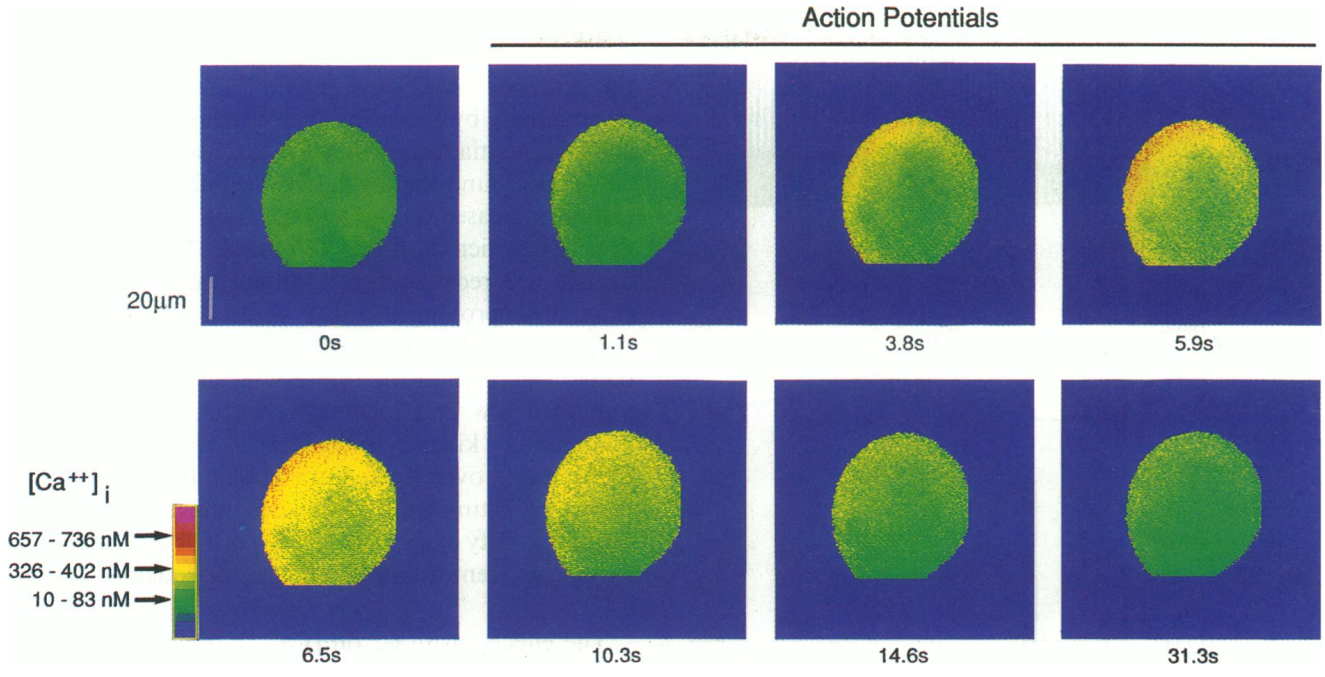

FIGURE 6 Profile of $[Ca^{++}]_i$ in an *Aplysia* sensory neuron cell body in response to action potential stimulation. Pseudocolor scale used is shown at lower left. $[Ca^{++}]_i$ range for representative color bins are indicated. 0 s: resting $[Ca^{++}]_i$ profile. 1.1–5.9 s: train of action potentials (indicated by bar) began at $t = 0.5$ s and ended at $t = 6.0$ s. During the train $[Ca^{++}]_i$ rose steeply near the outer rim of the cell and then diffused towards the center. 6.5 s: after the end of the stimulus $[Ca^{++}]_i$ continued to rise for a short time in the central areas of the cell due to inward diffusion of $[Ca^{++}]_i$. 10.3–31.3 s: $[Ca^{++}]_i$ gradually recovered towards rest. Images are pixel-by-pixel ratios of digitized images obtained with intensified CCD camera (Hamamatsu). Filter switching rate was 1.85 ratio measurements (wavelength pairs) per second. Stimulus train duration = 5.5 s, stimulus rate = 10 Hz, stimulus duration = 20 ms, current pulse = 1.6 nA.

same size frequently used in experiments. When the pinhole is placed by the outer rim of the model cell (Fig. 5 *B, left trace*), the $[Ca^{++}]_i$ transient time course more closely reflects the $[Ca^{++}]_i$ time course in the outermost shells (Fig. 1). Therefore, the peak amplitude is higher and the peak occurs just after the end of the current pulse. As the pinhole is moved inward to include shells primarily from the middle of the cell (Fig. 5 *B, middle* and *right traces*), the peak amplitude of the $[Ca^{++}]_i$ transient becomes smaller and occurs up to 1.5 s after the end of the current pulse. These effects are more pronounced with smaller pinholes. Similarly, the model also predicts that as the focal plane is moved from the center of the cell towards the top or bottom surface membrane, the $[Ca^{++}]_i$ transient peak amplitude will grow larger and occur with less delay (not shown).

COMPARISON OF EXPERIMENTAL $[Ca^{++}]_i$ RECORDINGS WITH THE MODEL

During a train of action potentials, Ca^{++} enters the cell through voltage-dependent Ca channels in the surface membrane giving rise to a transient increase in $[Ca^{++}]_i$. This $[Ca^{++}]_i$ transient was measured with fura-2 while focusing the microscope on a section through the center of an *Aplysia* sensory neuron cell body (Fig. 6). As in the model (Fig. 1), $[Ca^{++}]_i$ was seen to rise first and to the highest values near the rim of the cell just under the surface membrane (Fig. 6). In this particular cell there was a slight $[Ca^{++}]_i$ gradient even at rest with the highest values in the upper left part of the cell ($t = 0$ s). However, it can be seen that during the stimulus ($t = 1.1$ to 5.9) a steep gradient in $[Ca^{++}]_i$ was present from the rim to the center of the cell. Also, as in the model (Fig. 1), the peak value of $[Ca^{++}]_i$ at the rim of the cell coincided with the end of the stimulus (Fig. 6, $t = 5.9$ s), while the $[Ca^{++}]_i$ at the center of the cell did not reach its peak until 0.5 to 1.0 s after the end of the stimulus (Fig. 6, $t =$ 6.5 s). $[Ca^{++}]_i$ then gradually returned toward the resting prestimulus level (Fig. 6, $t = 10.3$, 14.6, 31.3 s). These results are in general agreement with measurements done in other cells (Lipscomb et al., 1988b; Hernandez-Cruz et al., 1989). However, unlike results from vertebrate sympathetic (Thayer et al., 1988a; Lipscombe et al., 1988a, b; Hernandez-Cruz et al., 1990) and sensory neurons (Thayer et al., 1988b) these cells showed no evidence of Ca^{++}-triggered Ca^{++} release from internal stores giving rise to a prolonged local elevation in $[Ca^{++}]_i$ lasting after the end of the stimulus (Hernandez-Cruz et al., 1990).

The delay from the end of the stimulus to the peak $[Ca^{++}]_i$ can be seen in PMT experiments as well. Fig. 7

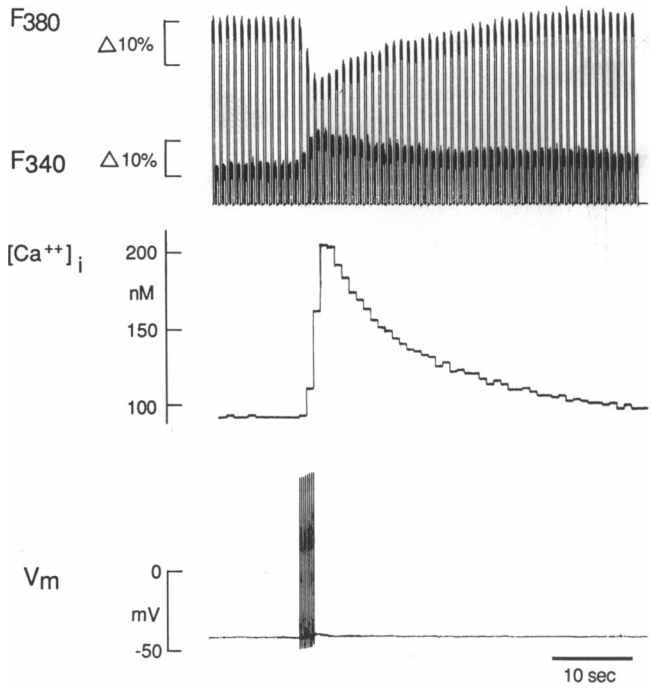

FIGURE 7 Example of a $[Ca^{++}]_i$ transient in an *Aplysia* sensory neuron cell body showing delay-to-peak of ~1.0 s following a train of action potentials. (*Bottom*) Membrane potential, V_m. Train duration = 1.6 s, stimulus rate = 5 Hz, stimulus duration = 5 ms, current pulse = 2.3 nA. (*Top*) Fura-2 fluorescence at 380 and 340 nm excitation measured as the filter changer alternated between the two wavelengths. The delay to peak is most easily seen in these single-wavelength measurements. The bottom of the fluorescence signal at each wavelength has been cut off; actual magnitude of 10% of the full amplitude of the fluorescence signals at each wavelength are indicated. Filter switching rate was 1.0 ratio measurements (wavelength pairs) per second. Diameter of pinhole aperture on PMT was 26 μm. Pinhole was centered ~15 μm from the edge of the cell. (*Middle*) $[Ca^{++}]_i$ calculated on-line from the ratio of background-subtracted fura-2 fluorescence signals at 340 and 380 nm.

shows a PMT recording with the pinhole position centered ~15 μm from the edge of the cell. The $[Ca^{++}]_i$ transient recorded in response to a train of action potentials has a similar time course to the simulated PMT measurements shown in Fig. 5 *B*. In addition, as in the simulated PMT measurements, $[Ca^{++}]_i$ continued to rise for ~1.0 s after the end of the action potential train. The model demonstrates that this delayed peak can be accounted for by continued diffusion of calcium towards the center of the cell after the end of the stimulus and disproportional weighting of the center of the cell by the recording apparatus.

RELIABILITY OF FURA-2 AS A $[Ca^{++}]_i$ INDICATOR

In addition to acting as a $[Ca^{++}]_i$ indicator, fura-2 is also a powerful Ca^{++} buffer which can diffuse throughout the cytoplasm (Grynkiewicz et al., 1985; Timmermann and Ashley, 1986). It is, therefore, important to investigate the effects of fura-2 itself on $[Ca^{++}]_i$. This was done experimentally by recording $[Ca^{++}]_i$ transients evoked by action potential trains in *Aplysia* sensory neurons (Fig. 8). It was found that as the intracellular fura-2 concentration increased due to leakage from a fura-2 filled intracellular microelectrode, (*a*) the $[Ca^{++}]_i$ transient amplitude was reduced, and (*b*) the recovery kinetics became more prolonged (Fig. 8 *A*). In a different cell (Fig. 8 *B*), where the intracellular microelectrode was partially clogged (and the fura-2 concentration, therefore, remained low and relatively constant) the amplitude and recovery kinetics of the $[Ca^{++}]_i$ transient were relatively stable over time. Intracellular fura-2 concentrations were estimated by comparing the absolute fluorescence intensity of the fura-2 in the cell to that of fura-2 at varying concentrations in a microelectrode cuvette (Fig. 8 *C*).

The effects of fura-2 on $[Ca^{++}]_i$ transients were also studied by varying the fura-2 concentration in the model (Fig. 9 *A*). The cross-sectional average $[Ca^{++}]_i$ was used here, and in much of what follows, since it was shown above to be very close to simulated PMT or video measurements (Fig. 5 *A*). In agreement with the PMT experimental results, the model predicts that increasing the fura-2 concentration should lead to a significant decrease in $[Ca^{++}]_i$ transient amplitude and a prolongation of recovery kinetics. An additional effect of fura-2, which is predicted by the model, is that fura-2 should speed up the net rate of $[Ca^{++}]_i$ diffusion in the cell. This is because fura-2, acting as a mobile $[Ca^{++}]_i$ buffer, will bind Ca^{++}, diffuse through the cell, and release Ca^{++} in areas with lower $[Ca^{++}]_i$. This can be seen in Fig. 1 where peak $[Ca^{++}]_i$ in the innermost shell of the model occurs 1.5 s after the end of the stimulus when 10 μM fura-2 is present (Fig. 1 *A*), but occurs just 0.6 s after the end of the stimulus when 50 μM fura-2 is present (Fig. 1 *B*). Furthermore, as increasing fura-2 concentration speeds up the diffusion of $[Ca^{++}]_i$ towards the center of the cell, this will also result in a shorter delay to the peak of the $[Ca^{++}]_i$ transient, as seen in Fig. 9 *A*.

An additional aspect of fura-2 measurements that was important to evaluate is how rapidly the dye is able to respond to fast changes in $[Ca^{++}]_i$. One way of estimating how quickly fura-2 responds to dynamic changes in $[Ca^{++}]_i$ is to examine the instantaneous values for $[CaFura_n]$ and $[FreeFura_n]$ generated by the nonequilibrium model (Eqs. 13 and 14). These values can be used together with the K_d of fura-2 to calculate a value for $[Ca_n]$, which represents the instantaneous value for $[Ca^{++}]_i$ "seen" by fura-2 as it equilibrates with the actual $[Ca^{++}]_i$. This is mathematically equivalent to using $[CaFura_n]$ and $[FreeFura_n]$ to calculate fluorescence at

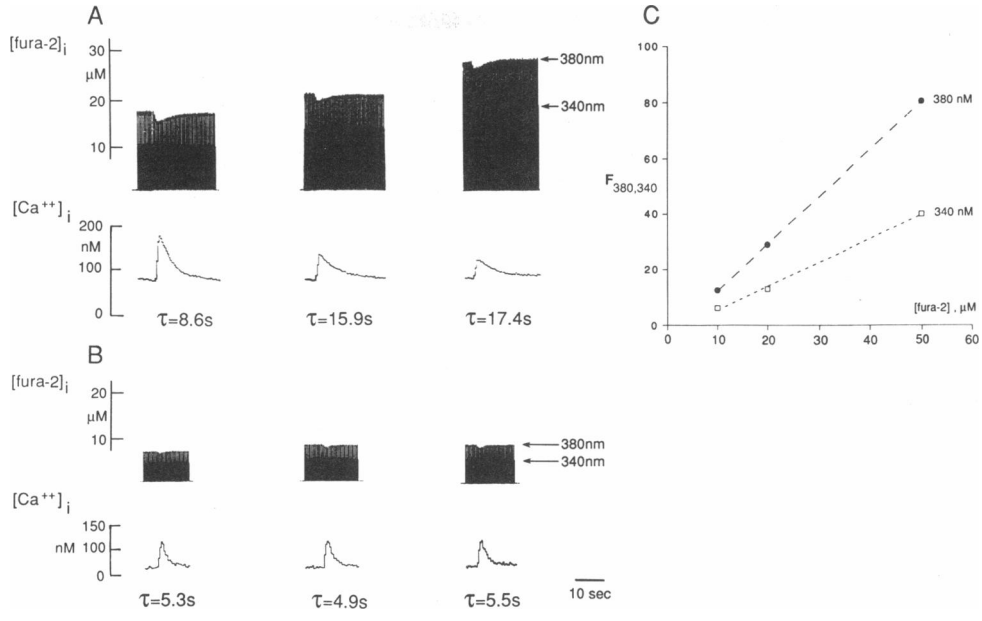

FIGURE 8 Effects of intracellular fura-2 concentration on $[Ca^{++}]_i$ signals in two *Aplysia* sensory neurons. (*A*) Intracellular fura-2 increasing over time. $[Ca^{++}]_i$ (*lower traces*) and absolute intensity of fura-2 fluorescence (*top traces*) at 340 and 380 nm excitation wavelengths are shown in response to a train of action potentials. The intracellular fura-2 concentration increased due to leakage from an intracellular fura-2 filled microelectrode. Middle trace was taken 13 min after left trace; Right trace was taken 27 min after left trace. Current pulse = 8.0 nA, stimulus duration = 2 ms, train duration = 2.0 s, stimulus rate = 5 Hz (10 action potentials). In *A*, *B*, and *C* diameter of pinhole aperture on PMT was 26 μm and filter switching rate was 1.0 ratio measurements (wavelength pairs) per second. (*B*) Intracellular fura-2 relatively low and constant. $[Ca^{++}]_i$ (*lower traces*) and absolute intensity of fura-2 fluorescence (*top traces*) at 340 and 380 nm excitation wavelengths in response to a train of action potentials. Middle trace was taken 16 min after left trace; right trace was taken 22 min after left trace. Current pulse = 5.6 nA, stimulus duration = 5 ms, train duration = 2.5 s, stimulus rate = 2 Hz (5 action potentials). (*C*) Estimation of $[Fura\text{-}2]_i$. Absolute fura-2 fluorescence levels ($F_{380,340}$, arbitrary units) are shown for microelectrodes filled with different fura-2 concentrations. Calibration bars for $[Fura\text{-}2]_i$ (*A* and *B*, *top traces*) were generated using the linear fit to the F_{380}, values shown here. Thus, the calibration bars for $[Fura\text{-}2]_i$ above refer to the fura-2 fluorescence intensities at 380 nm shown for the cells in the top traces. PMT pinhole aperture was focused on a region of the microelectrodes with a diameter similar to *Aplysia* sensory neurons (~50 μm). The solutions in the microelectrodes were calibration buffer (Blumenfeld et al., 1990) with $[Ca^{++}]$ = 100 nM, and [fura-2] as indicated.

340 and 380 nm using Eqs. 19–20, and then using the ratio of these values directly in Eq. 22 without incorporating the effects of microscope optics. The time course of fura-predicted $[Ca^{++}]_i$ calculated in this way was compared to the actual $[Ca^{++}]_i$ predicted by the model at very high time resolution (Fig. 9 *B*, *bottom* and *top traces*). With the onset of Ca^{++} influx, the nonequilibrium model predicts a steep initial rise in $[Ca^{++}]_i$ occurring before fura-2 and the cell's endogenous buffers begin to significantly buffer $[Ca^{++}]_i$. As buffering begins to occur, the $[Ca^{++}]_i$ rises steadily (Fig. 9 *B*, *top trace*), as does the fura-predicted $[Ca^{++}]_i$ (Fig. 9 *B*, *bottom trace*). At the end of the current pulse, $[Ca^{++}]_i$ has an initial steep decay (Fig. 9 *B*, *top trace*) due to the rapid equilibration of free Ca^{++} with fura-2 and endogenous buffer in the outermost shells. This is followed by a slower phase in which the time courses of $[Ca^{++}]_i$ and fura-predicted $[Ca^{++}]_i$ gradually converge. Note that the timecourse for $[Ca^{++}]_i$ predicted by the equilibrium model (Fig. 9 *B*, *middle trace*) lies between the nonequilibrium model and fura-predicted $[Ca^{++}]_i$. Thus, aside from an offset due to nonequilibrium conditions during the rising phase of $[Ca^{++}]_i$ transients, the model predicts that fura-2 should reliably detect $[Ca^{++}]_i$ to within a few milliseconds. This is well beyond the temporal resolution used in most fura-2 measurements.

EVALUATING POTENTIAL MECHANISMS OF $[Ca^{++}]_i$ TRANSIENT MODULATION

In presynaptic *Aplysia* sensory neurons, 5-HT increases and FMRFamide decreases the amplitude of action potential-induced $[Ca^{++}]_i$ transients, leading to corresponding changes in transmitter release (Klein and Kandel, 1978; Belardetti et al., 1987; Edmonds et al., 1990). Based on Arsenazo III and voltage clamp measurements, Boyle et al. (1984) suggested that 5-HT may increase $[Ca^{++}]_i$ transients both by increasing Ca^{++} influx and by altering intracellular calcium homeostasis. However, more recent experiments have suggested that 5-HT and FMRFamide modulate $[Ca^{++}]_i$ transients entirely through changes in Ca^{++} influx (Blumenfeld et al.,

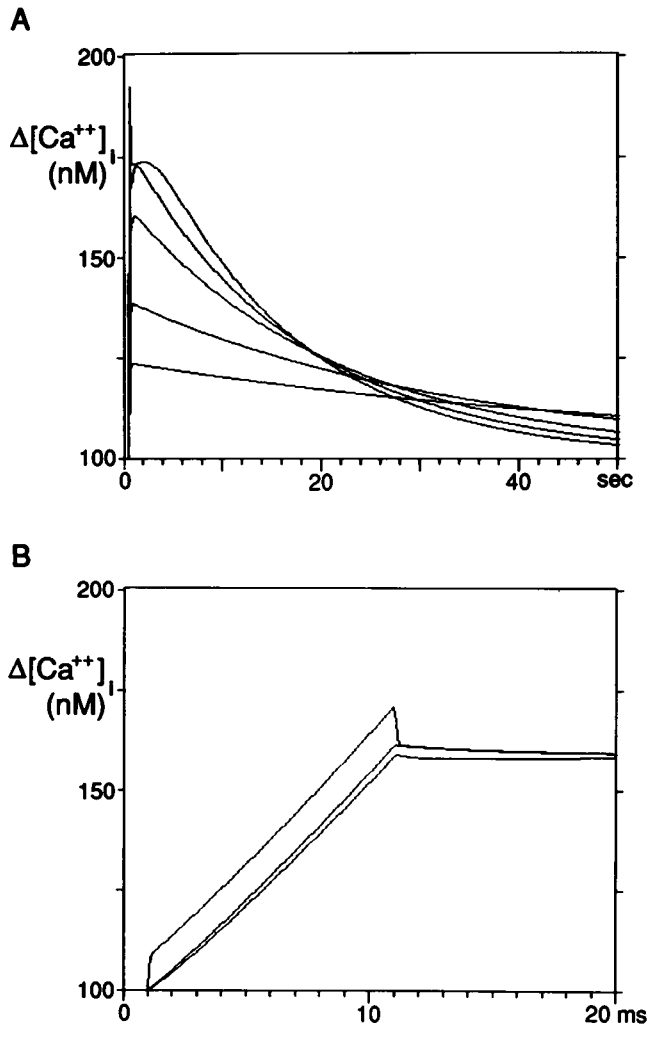

FIGURE 9 Simulation of effects of intracellular fura-2 on $[Ca^{++}]_i$ signals. (*A*) Effects of fura-2 concentration on $[Ca^{++}]_i$ transient amplitude and recovery kinetics. Average $[Ca^{++}]_i$ in a cross-section through the center of the model cell is shown in response to a single 10-ms current pulse with different fura-2 concentrations (from top to bottom): 0, 10, 20, 50, and 100 μM. Peak $[Ca^{++}]_i$ occurs with a delay of 1500, 900, 650, 500, and 450 ms, respectively, after the end of the stimulus. (*B*) Temporal fidelity of fura-2, and comparison of "equilibrium" and "nonequilibrium" models. High resolution time-course of average free calcium in a cross-section through the center of the model cell is shown in response to a 10-ms current pulse. (*Top trace*) $[Ca^{++}]_i$ predicted by "nonequilibrium" model using first order rate equations for binding of Ca^{++} to fura-2 and cellular buffer (Eqs. 8–14). (*Middle trace*) $[Ca^{++}]_i$ predicted by "equilibrium" model (Eq. 18). (*Bottom trace*) $[Ca^{++}]_i$ detected by fura-2, calculated from the values for $[Ca \cdot Fura_n]$ and $[FreeFura_n]$ generated by the nonequilibrium model for each time interval (see text). Fura-2 concentration is 10 μM. Similar results were obtained with 50 μM fura-2.

1990). Therefore, the model developed here was used to ask on theoretical grounds whether the $[Ca^{++}]_i$ transient modulation seen experimentally could be due to (*a*) changes in $[Ca^{++}]_i$ buffering or extrusion, (*b*) changes in Ca^{++} release from internal stores, or (*c*) changes in Ca^{++} influx.

1. Effects of Ca^{++} buffering and Ca^{++} transport

Increasing the concentration or affinity of intracellular Ca^{++} buffer in the model led to: (*a*) a decrease in $[Ca^{++}]_i$ transient amplitude, and (*b*) a prolongation of the recovery time course (Fig. 10, *A* and *B*). Decreasing $Ca^{++}{}_i$ buffering in the model had the opposite effects. Since 5-HT and FMRFamide modulate $[Ca^{++}]_i$ transient amplitude during action potentials without affecting the recovery time course (Boyle et al., 1984; Blumenfeld et al., 1990), this suggests that these transmitters do not act by changing intracellular Ca^{++} buffering.

When the fura-2 concentration in the model is increased from 10 μM (Fig. 10 *A*) to 50 μM (Fig. 10 *B*) the same changes in endogenous Ca^{++} buffering now have a smaller effect on both $[Ca^{++}]_i$ transient amplitude and recovery kinetics. Our measurements were all done with fura-2 concentrations below 50 μM. Therefore, we should have detected any changes in recovery kinetics produced by 5-HT or FMRFamide. If the fura-2 concentration had been significantly higher, however, fura-2 would dominate intracellular Ca^{++} buffering and pre-

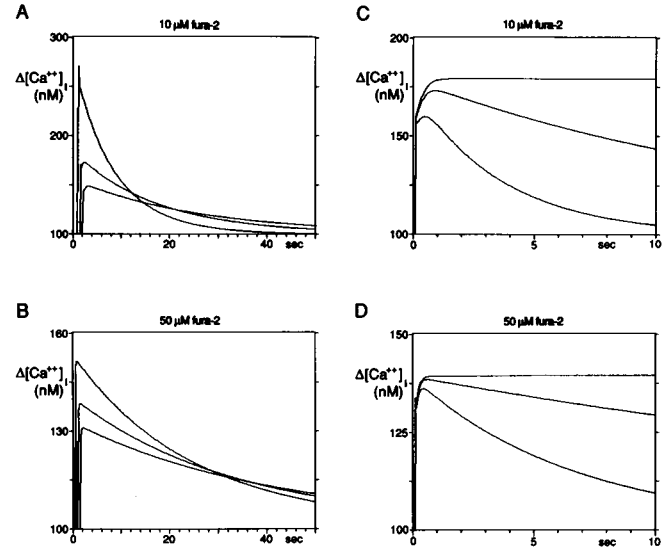

FIGURE 10 Effects of buffering and surface membrane pump on $[Ca^{++}]_i$ transients in the model cell. Timecourses of average $[Ca^{++}]_i$ are shown in a cross-section through the center of the model cell in response to a 10-ms current pulse. Fura-2 concentrations are indicated. (*A* and *B*) Effects of buffer concentration. (*Top traces*) Buffer concentration = 51 μM (β = 10). (*Middle traces*) Buffer concentration = 153 μM (β = 30). (*Bottom traces*) Buffer concentration = 255 μM (β = 50). Traces have been shifted slightly along the time axis for clarity of display. β is defined as $[Ca^{++}Buf]_i/[Ca^{++}]_i$ at rest. Identical results were obtained when intracellular calcium buffering was varied either by changing the buffer K_d or the buffer concentration, as long as β was varied by the same amount. In addition, in agreement with Sala et al. (1990), identical results were obtained whether K_d was varied by changing its forward or reverse rate constant. (*C* and *D*) Effects of surface membrane pump. Pump rate: P = 0/s (*top traces*); 20/s (*middle traces*); 100/s (*bottom traces*).

vent the detection of changes in endogenous Ca^{++} buffering.

As shown in Fig. 10, *C* and *D*, the model predicts that $[Ca^{++}]_i$ cannot return to resting values without a mechanism for calcium extrusion. Increasing the rate of the surface membrane pump speeds up the recovery kinetics of the $[Ca^{++}]_i$ transient, and slightly decreases its amplitude at the peak. Since neither 5-HT nor FMRFamide change $[Ca^{++}]_i$ transient recovery kinetics, this again implies that these transmitters probably do not significantly change $[Ca^{++}]_i$ homeostasis.

In both the models of Connor et al. (1982) and Sala et al. (1990), substantial recovery of $[Ca^{++}]_i$ occurs following a $[Ca^{++}]_i$ transient even when the pumping rate is zero. This discrepancy can be explained by different choices of buffer K_d and current amplitude which result in less saturation of cellular buffers near the surface membrane in our model. In contrast, in the other models, initial saturation of buffers near the surface membrane leads to a high initial free calcium which then decreases largely due to diffusion and redistribution of Ca^{++} to available buffers in the cytoplasm (Connor et al., 1982).

2. Ca^{++}-triggered Ca^{++} release from internal stores

If the relationship between the number of action potentials and $[Ca^{++}]_i$ transient amplitude were markedly nonlinear, this might suggest the presence of Ca^{++}-triggered Ca^{++} release from internal stores. In experiments with *Aplysia* sensory neurons it was found that, in fact, the $[Ca^{++}]_i$ transient amplitude increased approximately linearly with the number of action potentials in the train (Fig. 11, *A* and *B*). Our model was used to confirm that in the absence of Ca^{++}-triggered Ca^{++} release, the relationship between the number of Ca^{++} current pulses and $[Ca^{++}]_i$ transient amplitude is expected to be approximately linear (Fig. 11 *C*).

3. Modulation of Ca^{++} influx

We next asked whether or not the effects of 5HT and FMRFamide can be accounted for by modulation of Ca^{++} influx alone. The model was used to simulate PMT measurements of $[Ca^{++}]_i$ transients in response to a 1-s train of current pulses given at a frequency of 10 Hz (Fig. 11 *D*). The pulse duration was 3 ms and the current was varied to simulate changes in Ca^{++} influx. On this timescale, identical results were obtained if, instead, the current was kept constant and the pulse duration was varied to give the same changes in total charge movement. The relationship between $[Ca^{++}]_i$ transient amplitude and total charge movement per pulse shown in Fig. 11 *D* appears to be approximately linear (with a very slight upward concavity). As will be discussed further below, this result implies that modulation of Ca^{++} influx alone is of the correct magnitude to fully account for the changes in $[Ca^{++}]_i$ transient amplitude produced by 5-HT and FMRFamide.

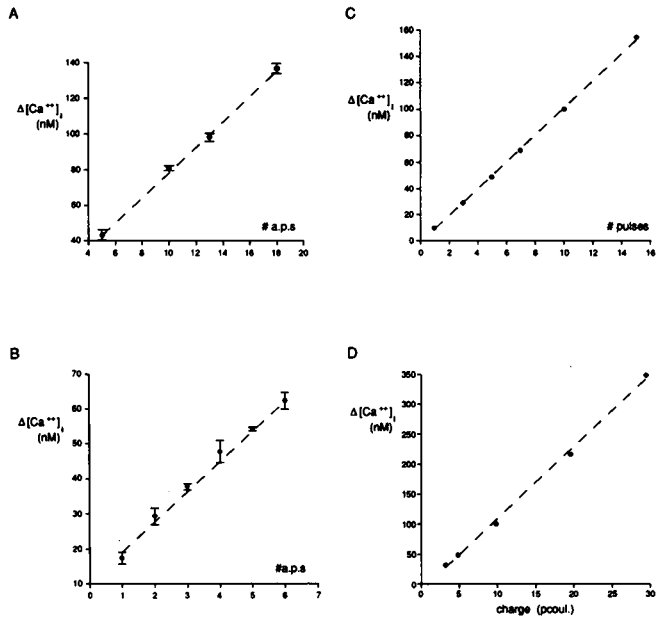

FIGURE 11 Experimental and theoretical relationships between Ca^{++} influx and $[Ca^{++}]_i$ transient amplitude. (*A, B, C*) Effect of number of action potentials or current pulses in the stimulus train. (*A, B*) Results of experiments in two different cells. Each point is the average $[Ca^{++}]_i$ transient amplitude (±SEM) for three trains with the indicated number of action potentials. Diameter of pinhole aperture on PMT was 26 μm, placed near the edge of the cell. Stimulus pulse rate, duration and current were 10 Hz, 20 ms, 4.2 nA (*A*); 2 Hz, 5 ms, 5.6 nA (*B*). (*C*) Theoretical relationship between number of pulses in train and $[Ca^{++}]_i$ transient amplitude in PMT measurements simulated with the model. PMT measurements were simulated as described in section on optical effects. Pinhole diameter = 26 μm, centered at 12 μm from middle of cell. Fura-2 concentration was 50 μM. Current density was 4.15×10^{-4} nA/cm^2 (3.23 nA). Pulse duration was 3 ms. Stimulus frequency was 10Hz. (*D*) Effect of Ca^{++} influx per pulse. Simulation of PMT measurements of $[Ca^{++}]_i$ in response to train of ten current pulses (pulse duration = 3 ms; frequency = 10 Hz; train duration = 1 s). The current per pulse was varied to give the charge per pulse (pcoul) indicated on the horizontal axis. Pinhole diameter = 16 μm, centered at 15 μm from middle of cell. Fura-2 concentration was 50 μM.

SUMMARY AND DISCUSSION

1. Interpretation of $[Ca^{++}]_i$ measurements with fura-2

The model described above enables a detailed analysis of the relationship between fura-2 measurements and the actual time-varying distribution of $[Ca^{++}]_i$ evoked in cells by Ca^{++} influx. Each stage in the signal pathway has been analyzed sequentially, from intracellular diffusion and buffering of Ca^{++}, to fura-2 and Ca^{++} binding, to the optical transfer function of the microfluorimetry system. Using this approach, it was possible to ask two general

questions about the fidelity of fura-2 measurements: (*a*) how closely do fura-2 measurements correspond to the actual $[Ca^{++}]_i$ in the cell?, and (*b*) how does fura-2 itself affect $[Ca^{++}]_i$?

According to the model, images obtained with fura-2 measurements are expected to be fairly close to the actual $[Ca^{++}]_i$ distribution in a cross-sectional focal plane of the cell. Thus, although a confocal microscope was not used, the contributions of out-of-focus light from above and below the focal plane are not expected to significantly distort the time-course of average $[Ca^{++}]_i$ in the focal plane. This may be explained by the partial confocal properties of fluorescence microscopy described by Hiraoka et al. (1990) when a field diaphragm of 100 μm or less is used, as it was in our measurements. Thus, the point spread function under these conditions decays to nearly zero within $\pm$ 5–6 μm of the focal plane, a distance over which $[Ca^{++}]_i$ does not vary in a major way for most choices of focal plane, except for near the surface membrane. The relatively fine depth of field implied by these measurements may also partly account for the recent impressive fura-2 images obtained from individual dendritic spines in the hippocampus without the use of confocal microscopy (Müller and Connor, 1991; Guthrie, Segal, and Kater, 1991).

At higher time resolution, during the rising phase of $[Ca^{++}]_i$ transients, the model predicts some discrepancies between the time course of fura-2 measurements and the actual $[Ca^{++}]_i$. During Ca^{++} influx, fura-2 will not be in equilibrium with $[Ca^{++}]_i$ in the outermost shells and, will therefore, underestimate $[Ca^{++}]_i$. Following this phase, however, the model predicts that the time course of actual $[Ca^{++}]_i$ and fura-2 measurements will be very similar. Thus, the temporal fidelity of fura-2 is expected to be adequate for the measurement of $[Ca^{++}]_i$ transients in the bulk cytoplasm in response to Ca^{++} influx. However, $[Ca^{++}]_i$, just under the surface membrane at high time resolution, which is thought to be most relevant for transmitter release at active zones (Smith and Augustine, 1988; Simon and Llinas, 1985), cannot be accurately recorded with fura-2 according to the model.

Since fura-2 is, itself, a $[Ca^{++}]_i$ buffer the model predicts that it should significantly decrease the amplitude and prolong the recovery kinetics of $[Ca^{++}]_i$ transients. These effects were seen in experiments as well, with intracellular fura-2 concentrations as low as 10 μM. Therefore, the intracellular fura-2 concentration should always be taken into account in experiments using fura-2. In addition, at intracellular fura-2 concentrations above $\sim$50 μM, the model predicts that fura-2 begins to dominate the endogenous buffers of the cell, making it difficult to detect changes in endogenous $[Ca^{++}]_i$ buffering. Therefore, for studies of the endogenous cellular $[Ca^{++}]_i$ buffering systems, intracellular fura-2 concentrations below $\sim$50 μM should be used. Finally, the model predicts that even low concentrations of fura-2 are expected to increase the rate of diffusion of calcium throughout the cell. This effect is probably somewhat exaggerated in our model since it does not incorporate other diffusible calcium buffers aside from fura-2. Nevertheless, care should be taken in interpreting experiments using fura-2 to measure the rate of intracellular calcium diffusion.

An apparent paradox is that fura-2 binding to calcium decreases the free calcium concentration and decreases the $[Ca^{++}]_i$ reported by fura-2, while, at the same time, the amount of calcium bound to fura-2 is increased. The explanation is that fura-2 measurements depend roughly on the ratio between bound fura-2 and free fura-2. Thus, although increasing the total fura-2 concentration will increase the bound fura-2, free fura-2 will increase even further, corresponding with the decrease in $[Ca^{++}]_i$.

2. Mechanisms of $[Ca^{++}]_i$ transient modulation

Aside from evaluating the reliability of fura-2 measurements, the second purpose of the model was to simulate several potential mechanisms for presynaptic modulation and to determine their expected effects on $[Ca^{++}]_i$ transients. Modulation of $[Ca^{++}]_i$ transients could, theoretically, occur through: (*a*) changes in $[Ca^{++}]_i$ homeostasis (e.g., $[Ca^{++}]_i$ buffering or transport); (*b*) changes in Ca^{++}-triggered release of Ca^{++} from internal stores; or (*c*) changes in Ca^{++} influx. Each of these three potential mechanisms was investigated with the model. The results of the model provide further support for previous experiments (Blumenfeld et al., 1990) that suggested that 5-HT and FMRFamide modulate $[Ca^{++}]_i$ transients in *Aplysia* sensory neurons entirely through changes in Ca^{++} influx.

As reported previously (Boyle et al., 1984; Blumenfeld et al., 1990), the recovery kinetics of $[Ca^{++}]_i$ transients are not altered by 5-HT or by FMRFamide. The model predicts that if changes in $[Ca^{++}]_i$ buffering or transport were used to modulate $[Ca^{++}]_i$ transient amplitude then there should be a significant change in recovery kinetics as well. However, opposing changes in both buffering and transport could, conceivably, modulate the $[Ca^{++}]_i$ transient amplitude with no net effect on recovery kinetics. Thus, according to the model, unless such counterbalancing effects are present, it is unlikely that changes in $[Ca^{++}]_i$ buffering or transport contribute to $[Ca^{++}]_i$ transient modulation in response to 5-HT or FMRFamide. Further evidence against the contribution of changes in $[Ca^{++}]_i$ homeostasis to modulation of $[Ca^{++}]_i$ transients has been provided by previous experiments in which $[Ca^{++}]_i$ transients evoked by Ca^{++} injections were not modulated by 5-HT or FMRFamide, while action potential-induced $[Ca^{++}]_i$ transients were modulated by both transmitters (Blumenfeld et al., 1990).

In sympathetic cells (Thayer et al., 1988a; Lipscombe et al., 1988a, b; Hernandez-Cruz et al., 1990) and DRG cells (Thayer et al., 1988b) it has been reported that Ca^{++}-triggered Ca^{++} release from internal stores gives

rise to a prolonged localized increase in $[Ca^{++}]_i$ lasting for several seconds after the end of a depolarizing stimulus. *Aplysia* sensory neurons do not exhibit this prolonged localized rise in $[Ca^{++}]_i$, however, it was found that in some cells the $[Ca^{++}]_i$ signal continued to increase for up to 1 s after the action potential train had terminated. The model was used to show that a delay of 1–2 s to the $[Ca^{++}]_i$ transient peak could be explained on the basis of Ca^{++} influx and diffusion alone if the region examined lay in a cross-section near the center of the cell. A number of different factors will influence this delay to peak. After the end of the action potential train, Ca^{++} continues to diffuse from the outermost shells, where $[Ca^{++}]_i$ is highest, toward the center of the cell. This was confirmed with video imaging of $[Ca^{++}]_i$ transients in *Aplysia* sensory neuron cell bodies. Thus, although $[Ca^{++}]_i$ falls after the end of the train in the few outermost shells, $[Ca^{++}]_i$ continues to rise in the many internal shells as it diffuses inward. These inner shells are weighted relatively more heavily in a cross-sectional average of calcium than in a volume average (Fig. 2 *inset*) and, therefore, the average $[Ca^{++}]_i$ taken in a cross-sectional focal plane continues to rise after the end of the train. If the measurements are done with a pinhole aperture placed near the center of the cell, the delay-to-peak will be exaggerated further (see Fig. 5 *B*). Therefore, a measured delay of 1 to 2 s to the $[Ca^{++}]_i$ transient peak after the end of Ca^{++} influx cannot be taken as evidence for Ca^{++}-triggered Ca^{++} release from internal stores.

Additional evidence against Ca^{++}-triggered Ca^{++} release from internal stores in *Aplysia* sensory neurons has come from experiments in which the number of action potentials in the stimulus train was found to be approximately linearly related to $[Ca^{++}]_i$ transient amplitude. A similar linear relationship was described by Smith and Zucker (1980) using Arsenazo III, and in rat DRG cells when Ca^{++} loads were in the range used here (Thayer and Miller, 1990). The actual Ca^{++} influx may not remain constant during successive action potentials in a train due to effects such as Ca channel inactivation and frequency-induced spike broadening. However, since $[Ca^{++}]_i$ increases by approximately the same amount with each successive action potential, these effects probably produce no net change in Ca^{++} influx (unless they are exactly offset by changes in $[Ca^{++}]_i$ homeostasis or release occuring during the train). The model was used to confirm that, in the absence of Ca^{++}-triggered Ca^{++} release, the relationship between the number of action potentials in the train and the $[Ca^{++}]_i$ transient amplitude is, in fact, expected to be approximately linear. This does not rule out the possibility of a linear Ca^{++} release process. However, even if Ca^{++}-induced Ca^{++} release were present it does not contribute to modulation of the action potential-induced $[Ca^{++}]_i$ transient. This conclusion is based on the lack of effect of 5-HT or FMRFa on $[Ca^{++}]_i$ transients evoked by Ca^{++} injections (Blumenfeld et al., 1990), which should contain a contribution from any Ca^{++}-induced Ca^{++} release process. One hypothetical mode of Ca^{++}-triggered Ca^{++} release which cannot be ruled out by these experiments would be release occurring just under the membrane in response to the very high local $[Ca^{++}]_i$. This type of Ca^{++}-triggered Ca^{++} release might not be triggered by Ca^{++} injections since the local submembrane $[Ca^{++}]_i$ may not be as high as during action potentials. It has been shown, however, that caffeine, which is known to induce Ca^{++}-triggered Ca^{++} release from internal stores in other neurons has no effect on $[Ca^{++}]_i$ in *Aplysia* sensory neurons (Blumenfeld et al., 1990).

The model was used to investigate whether changes in Ca^{++} influx alone can account for the modulation of $[Ca^{++}]_i$ transient amplitude observed experimentally. 5HT causes a 50% increase and FMRFamide a 40% decrease in the amplitude of $[Ca^{++}]_i$ transients produced by action potentials (Blumenfeld et al., 1990). Previous voltage clamp studies (Klein and Kandel, 1978; Belardetti et al., 1987; Edmonds et al., 1990) combined with recent Ca current modeling (Edmonds, 1990) have shown that 5HT increases and FMRFamide decreases total Ca^{++} current during action potentials by up to twofold. According to the model presented here, the relationship between Ca^{++} influx and $[Ca^{++}]_i$ transient amplitude is approximately linear. Therefore, the changes in Ca^{++} influx measured by voltage clamp are, alone, sufficient to produce the $[Ca^{++}]_i$ transient modulation seen with fura-2, without any need to invoke other mechanisms, such as changes in $[Ca^{++}]_i$ homeostasis or release.

It has recently been reported that 5-HT increases Ca^{++} influx during action potentials through two distinct mechanisms (Blumenfeld et al., 1991; Eliot et al., 1991). Based on experiments using 5-HT and dihydropyridines, about one-third of the increase in the $[Ca^{++}]_i$ transient is due to action potential broadening, while about two-thirds of the increase is due to direct modulation of a dihydropyridine-sensitive (L-type) calcium current. In the future, it should be possible to estimate the relative contributions of these two mechanisms for modulating the $[Ca^{++}]_i$ transient by using a Hodgkin-Huxley type Ca current model based on voltage clamp data together with the model presented here and to then compare this prediction to the imaging results obtained experimentally.

Thus, in agreement with prior experiments, the model provides additional evidence against changes in intracellular Ca^{++} buffering, transport, or release as mechanisms for modulating $[Ca^{++}]_i$ transients in response to 5-HT or FMRFamide. In addition, the model suggests that the modulation of Ca^{++} influx produced by 5-HT or FMRFamide should be sufficient to account for the observed modulation of $[Ca^{++}]_i$ transient amplitude produced by these transmitters.

3. Limitations of the model

As in previous models of $[Ca^{++}]_i$ diffusion (Blaustein and Hodgkin, 1969; Baker et al., 1971; Andresen et al., 1979; Smith and Zucker, 1980; Gorman and Thomas, 1980;

Connor and Nikolakopoulou, 1982; Zucker and Stockbridge, 1983; Fischmeister and Horackova, 1983; Stockbridge and Moore, 1984; Chad and Eckert, 1984; Simon and Llinas, 1985; Zucker and Fogelson, 1986; Gamble and Koch, 1987; Parnas et al., 1989; Holly and Poledna, 1989; Sala et al., 1990; Dissing et al., 1990; Holmes and Levy, 1990) our model is limited by the incomplete information available for several model parameters. Most importantly, the exact properties of neuronal $[Ca^{++}]_i$ buffers and extrusion mechanisms have not been fully characterized. The values used in our model for $[Ca^{++}]_i$ buffering and extrusion are based on the available experimental estimates for these parameters (e.g., Requena and Mullins, 1979; DiPolo and Beauge, 1983; Blaustein et al., 1978; Ahmed and Connor, 1988; Schatzmann, 1989; Carafoli, 1987; Blaustein, 1989) and the Ca current values are based on voltage clamp measurements (Edmonds et al., 1990). The spatial and temporal characteristics of the $[Ca^{++}]_i$ transients that we simulated in this manner are in reasonable agreement with experiments in *Aplysia* sensory neurons, however the model parameters could be further adjusted in a variety of ways in order to get a better fit. Thus, while the current set of model parameters give simulations which approximate the experimental results, they do not represent an optimal fit to the empirical data.

In addition, there are a number of factors that have been neglected by the model, which may significantly influence $[Ca^{++}]_i$ transients in real cells. Thus, for example, in our model we have included a single, uniformly distributed, immobile $[Ca^{++}]_i$ buffer, while in cells, multiple $[Ca^{++}]_i$ buffers are present, some of which are thought to be mobile in the cytoplasm (Carafoli, 1987; Blaustein, 1988). In addition, there is evidence that subcellular inhomogeneities in buffering may alter local $[Ca^{++}]_i$ (Tillotson and Gorman, 1980). Calcium influx is also likely to be nonuniform in neurons (Anglister et al., 1982; Connor, 1986; Smith and Augustine, 1988; Thompson and Coombs, 1988; Tank et al., 1988; Hockberger et al., 1989; Blumenfeld et al., 1990; Silver et al., 1990). Although the $[Ca^{++}]_i$ extrusion mechanism in our model is restricted to the surface membrane, Ca^{++}-ATPase pumps located on endoplasmic reticulum are likely to play a significant role in removal of $[Ca^{++}]_i$ as well (Blaustein et al., 1978; Blaustein, 1988). Finally, the presence of cytoskeletal elements, intracellular organellar membranes, and invaginations of the surface membrane (Mirolli and Talbott, 1972; Graubard, 1975) may also significantly alter the influx and diffusion of $[Ca^{++}]_i$. Despite its limitations, this model provides important information about the reliability of fura-2 microfluorescence measurements, and, in addition, allows further insight into potential mechanisms for modulation of $[Ca^{++}]_i$ transients in *Aplysia* sensory neurons.

We gratefully acknowledge the support and advice of Steven A. Siegelbaum in whose laboratory this work was done. We thank Gareth Tibbs for helpful comments on the manuscript and John A. Connor for reviewing a preliminary draft of this work. We also thank Charles L. Lam for preparing the figures.

Received for publication 27 January 1992 and in final form 26 May 1992.

REFERENCES

Abrams, T. W., V. F. Castellucci, J. S. Camardo, E. R. Kandel, and P. E. Lloyd. 1984. Two endogenous neuropeptides modulate the gill and siphon withdrawal reflex in *Aplysia* by presynaptic facilitation involving cAMP-dependent closure of a serotonin-sensitive potassium channel. *Proc. Natl. Acad. Sci. USA.* 81:7956–7960.

Adler, E. M., G. J. Augustine, S. N. Duffy, and M. P. Charlton. 1991. *J. Neurosci.* 11:1496–1507.

Ahmed, Z., and J. A. Connor. 1988. Calcium regulation by and buffer capacity of molluscan neurons during calcium transients. *Cell Calcium.* 9:57–69.

Andresen, M. C., A. M. Brown, and S. Yasui. 1979. The role of diffusion in the photoresponse of an extraretinal photoreceptor of *Aplysia. J. Physiol. (Lond.).* 287:283–301.

Anglister, L., I. C. Farber, A. Shahar, and A. Grinvald. 1982. Localization of voltage-sensitive calcium channels along developing neurites: their possible role in regulating neurite elongation. *Dev. Biol.* 94:351–365.

Baker, P. F., A. L. Hodgkin, and E. B. Ridgway. 1971. Depolarization and calcium entry in squid giant axons. *J. Physiol. (Lond.).* 218:709–755.

Barish, M. E., and S. H. Thompson. 1983. Calcium buffering and slow recovery kinetics of calcium-dependent outward current in molluscan neurones. *J. Physiol. (Lond.).* 337:201–219.

Belardetti, F., E. R. Kandel, and S. A. Siegelbaum. 1987. Neuronal inhibition by the peptide FMRFamide involves opening of S K^+ channels. *Nature (Lond.).* 325:153–156.

Blaustein, M. P. 1988. Calcium transport and buffering in neurons. *TINS.* 11:438–443.

Blaustein, M. P., and A. L. Hodgkin. 1969. The effect of cyanide on the efflux of calcium from squid axons. *J. Physiol. (Lond.).* 200:497–527.

Blaustein, M. P., R. W. Ratzlaff, and E. S. Schweitzer. 1978. Calcium buffering in presynaptic nerve terminals. *J. Gen. Physiol.* 72:43–66.

Blumenfeld, H., L. S. Eliot, B. W. Edmonds, E. R. Kandel, and S. A. Siegelbaum. 1991. 5-HT increases Ca^{++} influx during action potentials in *Aplysia* sensory neurons by spike broadening and by direct calcium channel modulation. *Soc. Neurosci. Abs.* 17:1485.

Blumenfeld, H., M. E. Spira, E. R. Kandel, and S. A. Siegelbaum. 1990. Facilitatory and inhibitory transmitters modulate calcium influx during action potentials in *Aplysia* sensory neurons. *Neuron.* 5:487–499.

Boyle, M. B., M. Klein, S. J. Smith, and E. R. Kandel. 1984. Serotonin increases intracellular Ca^{++} transients in voltage-clamped sensory neurons of *Aplysia californica. Proc. Natl. Acad. Sci. USA.* 81:7642–7646.

Brezina, V., R. Eckert, and C. Erxleben. 1987. Modulation of potassium conductances by an endogenous neuropeptide in neurones of *Aplysia californica. J. Physiol. (Lond.).* 382:267–290.

Bronstejn, I. N., and K. A. Siemiendiajew. 1959. Handbook Encyclopedia of Mathematics. Government Scientific Publishers, Warsaw. 162–163.

Carafoli, E. 1987. Intracellular calcium homeostasis. *Annu. Rev. Biochem.* 56:395–433.

Chad, J. E., and R. Eckert. 1984. Calcium domains associated with individual channels can account for anomalous voltage relations of Ca-dependent responses. *Biophys. J.* 45:993–999.

Connor, J. A., and Nikolakopoulou. 1982. Calcium diffusion and buffering in nerve cytoplasm. *Lect. Math. Life Sci.* 15:79–101.

Connor, J. A., R. Kretz, and E. Shapiro. 1986. Calcium levels measured in a presynaptic neurone of *Aplysia* under conditions that modulate transmitter release. *J. Physiol.* 375:625–642.

DiPolo, R., and L. Beauge. 1983. The calcium pump and sodium-calcium-exchange in squid axons. *Annu. Rev. Physiol.* 45:313–324.

Dissing, S., B. Nauntofte, and O. Sten-Knudsen. 1990. Spatial distribution of intracellular, free Ca^{2+} in isolated rat parotid acini. *Pflügers Arch., Eur. J. Physiol.* 417:1–12.

Edmonds, B. 1990. Contributions of two classes of calcium channels to transmitter release and plasticity in the sensory neurons of *Aplysia*. Doctoral dissertation. University Microfilms International, Ann Arbor, Michigan.

Edmonds, B., M. Klein, N. Dale, and E. R. Kandel. 1990. Contributions of two types of calcium channels to synaptic transmission and plasticity. *Science (Wash. DC)*. 250:1142–1147.

Eliot, L. S., H. Blumenfeld, B. W. Edmonds, E. R. Kandel, and S. A. Siegelbaum. 1991. Imaging $[Ca]_i$ transients at *Aplysia* sensorimotor synapses: contributions of direct and indirect modulation to presynaptic facilitation. *Soc. Neurosci. Abs.* 17:1485.

Fay, F. S., W. Carrington, and K. E. Fogarty. 1989. Three-dimensional molecular distribution in single cells analyzed using the digital imaging microscope. *J. Microscopy.* 153:133–149.

Fay, F. S., K. E. Fogarty, and J. M. Coggins. 1986. Analysis of molecular distribution in single cells using a digital imaging microscope. *In* Optical Methods in Cell Physiology. P. DeWeer and B. M. Salzberg, editors. Wiley-Interscience, New York.

Fischmeister, R., and M. Horackova. 1983. Variation of intracellular Ca^{2+} following Ca^{2+} current in heart. *Biophys. J.* 41:341–348.

Gamble, E., and C. Koch. 1987. The dynamics of free calcium in dendritic spines in response to repetitive synaptic input. *Science (Wash. DC)*. 236:1311–1315.

Gorman, A. L. F., and M. V. Thomas. 1980. Intracellular calcium accumulation during depolarization in a molluscan neurone. *J. Physiol. (Lond.)*. 308:259–285.

Graubard, K. 1975. Voltage attenuation within *Aplysia* neurons: the effect of branching pattern. *Brain Res.* 88:325–332.

Grynkiewicz, G., M. Poenie, and R. Y. Tsien. 1985. A new generation of Ca^{++} indicators with greatly improved fluorescence properties. *J. Biol. Chem.* 260:3440–3450.

Guthrie, P. B., M. Segal, and S. B. Kater. 1991. Independent regulation of calcium revealed by imaging of dendritic spines. *Nature (Lond.)*. 354:76–79.

Hecht, E., and A. Zajac. 1974. Optics. Addison-Wesley.

Hernandez-Cruz, A., F. Sala, and P. R. Adams. 1989. Subcellular dynamics of $[Ca^{++}]_i$ monitored with laser scanned confocal microscopy in a single voltage-clamped vertebrate neuron. *Biophys. J.* 55:216*a*. (Abstr.)

Hernandez-Cruz, A., F. Sala, and P. R. Adams. 1990. Subcellular calcium transients visualized by confocal microscopy in a voltage-clamped vertebrate neuron. *Science (Wash. DC)*. 247:858–862.

Hiraoka, Y., J. W. Sedat, and D. A. Agard. 1990. Determination of three-dimensional imaging properties of a light microscope system. *Biophys. J.* 57:325–333.

Hochner, B., M. Klein, S. Schacher, and E. R. Kandel. 1986. Action-potential duration and the modulation of transmitter release from the sensory neurons of *Aplysia* in presynaptic facilitation and behavioral sensitization. *Proc. Natl. Acad. Sci. USA.* 83:8794–8798.

Hockberger, P. E., H. Y. Tseng, and J. A. Connor. 1989. Fura-2 measurements of cultured rat Purkinje neurons show dendritic localization of Ca^{++} influx. *J. Neurosci.* 9:2272–2284.

Holly, M., and J. Poledna. 1989. Model of calcium diffusion, binding and membrane transport in the sarcomere of frog skeletal muscle. *Gen. Physiol. Biophys.* 8:539–553.

Holmes, W. R., and W. B. Levy. 1990. Insights into associative long-term potentiation from computational models of NMDA receptor-mediated calcium influx and intracellular calcium concentration changes. *J. Neurophysiol.* 63:1148–1168.

Hopkins, H. H. 1955. The frequency response of a defocused optical system. *Proc R. Soc. (Lond.)*. A231:91–103.

Inoue, S. 1986. Video Microscopy. Plenum Press, New York.

Jackson, A. P., M. P. Timmermann, C. R. Bagshaw, and C. C. Ashley. 1987. The kinetics of calcium binding to fura-2 and indo-1. *Fed. Eur. Biochem. Soc. Lett.* 216:35–39.

Kandel, E. R., and J. H. Schwartz. 1982. Molecular biology of learning: modulation of transmitter release. *Science (Wash. DC)*. 218:433–443.

Klein, M., and E. R. Kandel, 1978. Presynaptic modulation of voltage-dependent Ca^{++} current: mechanism for behavioral sensitization in *Aplysia californica. Proc. Natl. Acad. Sci. USA.* 75:3512–3516.

Konishi, M., A. Olson, S. Hollingworth, and S. M. Baylor. 1988. Myoplasmic binding of fura-2 investigated by steady-state fluorescence and absorbance measurements. *Biophys. J.* 54:1089–1104.

Lipscombe, D., D. V. Madison, M. Poenie, H. Reuter, R. W. Tsien, and R. Y. Tsien. 1988a. Imaging of cytosolic Ca^{++} transients arising from Ca^{++} stores and Ca^{++} channels in sympathetic neurons. *Neuron.* 1:355–365.

Lipscombe, D., D. V. Madison, M. Poenie, H. Reuter, R. Y. Tsien, and R. W. Tsien. 1988b. Spatial distribution of calcium channels and cytosolic calcium transients in growth cones and cell bodies of sympathetic neurons. *Proc. Natl. Acad. Sci. USA* 85:2398–2402.

Mirolli, M., and S. Talbott. 1972. The geometrical factors determining the electronic properties of a molluscan neuron. *J. Physiol.* 227:19–34.

Müller, W., and J. A. Connor. 1991. Dendritic spines as individual neuronal compartments for synaptic Ca^{2+} responses. *Nature (Lond.)*. 354:73–76.

Parnas, H., G. Hovav, and I. Parnas. 1989. Effect of Ca^{2+} diffusion on the time course of neurotransmitter release. *Biophys. J.* 55:859–874.

Requena, J., and L. J. Mullins. 1979. Calcium movement in nerve fibres. *Quart. Rev. Biophys.* 12:371–460.

Sala, F., and A. Hernandez-Cruz. 1990. Calcium diffusion modeling in a spherical neuron. *Biophys. J.* 57:313–324.

Schatzmann, H. J. 1989. The calcium pump of the surface membrane and of the sarcoplasmic reticulum. *Annu. Rev. Physiol.* 51:473–485.

Sheppard, C. J. R. 1988. Depth of field in optical microscopy. *J. Microscopy.* 149:73–75.

Siegelbaum, S. A., J. S. Camardo, and E. R. Kandel. 1982. Serotonin and cyclic AMP close single K+ channels in *Aplysia* sensory neurones. *Nature (Lond.)*. 299:413–417.

Silver, R. A., A. G. Lamb, and S. R. Bolsover. 1990. Calcium hotspots caused by L-channel clustering promote morphological changes in neuronal growth cones. *Nature (Lond.)*. 343:751–754.

Simon, S. M., and R. R. Llinas. 1985. Compartmentalization of the submembrane calcium activity during calcium influx and its significance in transmitter release. *Biophys. J.* 48:485–498.

Smith, S. J., and G. J. Augustine. 1988. Calcium ions, active zones and synaptic transmitter release. *Trends Neurosci.* 11:458–464.

Smith, S. J., and R. S. Zucker. 1980. Aequorin response facilitation and

intracellular calcium accumulation in molluscan neurones. *J. Physiol. (Lond.)*. 300:167–196.

Stockbridge, N., and J. W. Moore. 1984. Dynamics of intracellular calcium and its possible relationship to phasic transmitter release and facilitation at the frog neuromuscular junction. *J. Neurosci.* 4:803–811.

Stockseth, P. A. 1969. Properties of a defocused optical system. *J. Optical Soc. Am.* 59:1314–1321.

Strautman, A. F., J. R. Cork, and K. R. Robinson. 1990. The distribution of free calcium in transected spinal axons and its modulation by applied electrical fields. *J. Neurosci.* 10:3564–3575.

Tank, D. W., M. Sugimori, J. A. Connor, and R. R. Llinas. 1988. Spatially resolved calcium dynamics of mammalian Purkinje cells in cerebellar slice.

Thayer, S. A., L. D. Hirning, and R. J. Miller. 1988a. The role of caffeine-sensitive calcium stores in the regulation of the intracellular free calcium concentration in rat sympathetic neurons in vitro. *Mol. Pharmacol.* 34:664–673.

Thayer, S. A., and R. J. Miller. 1990. Regulation of the intracellular free calcium concentration in single rat dorsal root ganglion neurones in vitro. *J. Physiol.* 425:85–115.

Thayer, S. A., T. M. Perney, and R. J. Miller. 1988b. Regulation of calcium homeostasis in sensory neurons by bradykinin. *J. Neurosci.* 8:4089–4097.

Thompson, S. H., and J. Coombs. 1988. Spatial distribution of Ca currents in molluscan neuron cell bodies and regional differences in the strength of inactivation. *J. Neurosci.* 8:1929–1939.

Tillotson, D., and A. L. F. Gorman. 1980. Non-uniform Ca^{2+} buffer distribution in a nerve cell body. *Nature (Lond.)*. 286:816–817.

Timmermann, M. P., and C. C. Ashley. 1986. Fura-2 diffusion and its use as an indicator of transient free calcium changes in single striated muscle cells. *Fed. Eur. Biochem. Soc. Lett.* 209:1–8.

Williams, D. A., K. E. Fogarty, R. Y. Tsien, and F. S. Fay. 1985. Calcium gradients in single smooth muscle cells revealed by the digital imaging microscope using fura-2. *Nature (Lond.)*. 318:558–561.

Zucker, R. S., and A. L. Fogelson. 1986. Relationship between transmitter release and presynaptic calcium influx when calcium enters through discrete channels. *Proc. Natl. Acad. Sci. USA.* 83:3032–3036.

Zucker, R. S., and N. Stockbridge. 1983. Presynaptic Calcium diffusion and the time courses of transmitter release and synaptic facilitation at the squid giant synapse. *J. Neurosci.* 3:1263–1269.